# Extension of the Sussman-Bathe spline-based hyperelastic model to incompressible transversely isotropic materials

Marcos Latorre, Francisco Javier Montáns

*Escuela Técnica Superior de Ingenieros Aeronáuticos, Universidad Politécnica de Madrid*
*Pza.Cardenal Cisneros, 28040-Madrid, Spain*

**Abstract**

In this paper we extend the Sussman-Bathe spline-based hyperelastic isotropic model to predict the behavior of transversely isotropic isochoric materials. The model is based on an uncoupled decomposition of the stored energy function and a generalization of the inversion formula used by Sussman and Bathe. The present extension introduces some approximations that, in all studied cases, do not yield relevant deviations from the experimental data. The isotropic model results in a particular case of the present formulation. Several possibilities of user-prescribed experimental data are addressed. The model is used to predict experiments of calendered rubber and of biological tissues.

*Keywords:* Hyperelasticity; nonlinear elasticity; incompressible materials; transverse isotropy; living tissues; rubber-like materials.

*Email addresses:* m.latorre.ferrus@upm.es (Marcos Latorre), fco.montans@upm.es (Francisco Javier Montáns)

## 1. Introduction

As it is well known, in the stress and strain analysis of solids there are important practical consequences when considering large deformations. Whereas at small strains the constitutive equations for elastic behavior are simply obtained from the determination of some constants that linearly relate stress and strain components, at large strains the situation is considerably more complex [1]. Materials that achieve large (or moderate) elastic strains behave in a nonlinear manner [2]. Polymers [3] and biological tissues [4] are just some examples. For metals elastic behavior is frequently considered linear in elastoplastic models when using logarithmic stress and strain measures [5],[6], but nonlinear when using other strain measures. In order to account for such nonlinearity, specially in computational elastoplasticity, initial formulations for finite element implementation used objective rate (incremental) forms in which the material parameters where constant or a function of the strain state. Stress integration was complex in order to preserve objectivity. In elasto-plasticity, the Rolph-Bathe [7] and Hughes-Winget [8] algorithms are just two examples. As shown by Simó and Pister [9], these formulations are not truly elastic (hence hypoelastic), and energy is not preserved during closed cycles [2]. In order to be elastic, the elastic tensor at large strains has to fulfill some compatibility conditions, apart from full symmetry [10]. Those conditions are automatically accomplished if the constitutive equation is directly obtained from a known stored energy expression or model.

Many such models exist in the literature aimed at the prediction of the

behavior of different materials. The Ogden [11], Mooney-Rivlin [12][13], Arruda-Boyce [14], Blatz-Ko [15] and Yeoh [16] models are some of the best known. These models have a given "shape" and some parameters to be determined from a best fit of the experimental data for a given range of expected strains. In a practical problem, the engineer must select the model and the strain range. If fortunate, the predicted behavior may capture the global behavior, but it may miss some finer (probably important) details. Thus one may wonder if having an error on the preserved energy is more important than having an error on the stress-strain behavior if the problem is not of repeated cyclic loading type, sacrifying accuracy for physical and mathematical correctness. Furthermore, what an analyst would like is to just prescribe some stress-strain points and automatically obtain a predicted behavior consistent with the prescribed data. In that sense, there is a temptation to go back to hypoelastic formulations.

A solution to this dilemma has been recently given by Sussman and Bathe [17]. In their work they propose the use of splines to model the stress-strain behavior. The splines are computed such that they pass through experimental stress-strain points and have the desired continuity. Hence, they "exactly" capture the experimental data. Stresses are then expressed in terms of those splines. The key point of their paper is that whereas these initial interpolating splines are not derived from a stored energy function (and hence the behavior is not hyperelastic), the relationship may be inverted. A new set of functions is obtained, which still pass through the experimental data and

that is derived from a stored energy function (hence the behavior is hyperelastic). Furthermore, computational efficiency is not a relevant issue because the domain of the new set may be divided into equally spaced subdomains so the location within the desired subdomain is a simple operation. The model is a genuine case of WYPIWYG (What You *Prescribe* is What You Get) philosophy which is still physically and mathematically correct.

The Sussman-Bathe model is valid for isotropic hyperelasticity. The purpose of the present work is to extend the model for transversely isotropic materials, as for example some fiber composites, rubber-like materials or biological tissues. We consider the incompressible case, which of course may be extended to the quasi-incompressible case through a volumetric stored energy. Unlike the isotropic model, several cases need to be considered, each case for a given set of possible experimental data. We address those cases in the following sections and also consider isotropy as a special case. Some predictions for actual experiments taken from the literature are presented.

The outline of the paper is as follows. In the following section we review some concepts and procedures essential in our formulation ("building blocks"). Then we can easily introduce the actual procedure on these footings, taking into consideration several possible sets of experiments to obtain the needed data. In the fourth section we show some examples.

## 2. Building blocks

In this section we briefly review some concepts and formulations that we will use in the procedure outlined in the following section. Once these building blocks are explained and understood, the procedure is relatively simple.

### *2.1. Splines based piecewise interpolation used in the model*

Assume that during a tensile test (or any other test), we have obtained some experimental data given by $N+1$ points of a stress-strain behavior $(y_i \equiv \tilde{\sigma}_i,\ x_i \equiv \tilde{E}_i)$, $i = 1, ..., N+1$ in any defined stress and strain measure. We are interested in the interpolation of such data with a given degree of smoothness, see Figure 1. A handy well known method (specially in CAD) is the use of splines. In our case we will use piecewise cubic splines. In essence the method consists on fitting a third order polynomial between two points such that the slope $y'(x = x_i) \equiv Y_i$ and the derivative of the slope $y''(x = x_i) \equiv Y_i'$ are also the same at both sides of each experimental point. Physically, as seen below, this means that we wish the moduli and its derivative to be continuous, which are attractive smoothness requirements for hyperelastic behavior. In order to obtain the usual tridiagonal system of equations, each subdomain is normalized to $\xi = (x - x_i) / (x_{i+1} - x_i) \in [0, 1]$ so all $N$ polynomia have the expression

$$P_i(\xi \in [0, 1]) = a_i + b_i\xi + c_i\xi^2 + d_i\xi^3 \tag{1}$$

For each subdomain, the conditions $y_i = P_i(0)$, $y_{i+1} = P_i(1)$, are given, where $y_i$ are the known experimental data. Between any two subdomains, two additional conditions are established

$$P'_{i-1}(1) = P'_i(0) =: Y_i \tag{2}$$

$$P''_{i-1}(1) = P''_i(0) \;\Rightarrow\; 2c_{i-1} + 6d_{i-1} = 2c_i \tag{3}$$

where $Y_i$ are also unknowns. However, using (1) and (2), for each subdomain it is straightforward to verify that

$$\begin{cases} a_i = y_i \quad (= P_i(0)) \\ b_i = Y_i \quad (= P'_i(0)) \\ c_i = 3(y_{i+1} - y_i) - 2Y_i - Y_{i+1} \quad (= P''_i(0)/2) \\ d_i = 2(y_i - y_{i+1}) + Y_i + Y_{i+1} \quad (= P'''_i/6) \end{cases} \tag{4}$$

so the $Y_i$ may be used as basic variables and Eq. (3) results for each subdomain in

$$Y_{i-1} + 4Y_i + Y_{i+1} = 3(y_{i+1} - y_{i-1}) \tag{5}$$

Only the first and last $Y_i$ cannot be determined with this set of equations. A usual ("natural") choice to obtain the additional equations is to set $P''_1(0) = 0$ and $P''_N(1) = 0$ in Eq. (3), where $N$ is the number of subdomains. Then

the following tridiagonal system of $N+1$ equations is obtained

$$\begin{bmatrix} 2 & 1 & & & \\ 1 & 4 & 1 & & \\ & & \ldots & & \\ & & 1 & 4 & 1 \\ & & & 1 & 2 \end{bmatrix} \begin{bmatrix} Y_1 \\ Y_2 \\ \ldots \\ Y_N \\ Y_{N+1} \end{bmatrix} = \begin{bmatrix} 3\left(y_2 - y_1\right) \\ 3\left(y_3 - y_1\right) \\ \ldots \\ 3\left(y_{N+1} - y_{N-1}\right) \\ 3\left(y_{N+1} - y_N\right) \end{bmatrix} \tag{6}$$

which can be efficiently solved using the TDMA (Thomas) algorithm, well known in the CFD literature. Obviously, other boundary conditions may be applied.

*2.2. Assumed uncoupled decomposition of the stored energy function*

The model is motivated by the widely accepted Valanis-Landel hypothesis [18] which we briefly review and extend to transversely isotropic materials. Let ${}^0\boldsymbol{x}$ be the coordinates of a material point at a reference time (material configuration) and ${}^t\boldsymbol{x}$ the coordinates at time $t$. Using the notation given in References [1][2], the deformation gradient is

$${}^t_0\boldsymbol{X} = \frac{\partial\, {}^t\boldsymbol{x}}{\partial\, {}^0\boldsymbol{x}} = {}^t_0\boldsymbol{R}\, {}^t_0\boldsymbol{U} = {}^t_0\boldsymbol{V}\, {}^t_0\boldsymbol{R} \tag{7}$$

where ${}^t_0\boldsymbol{R}$ and ${}^t_0\boldsymbol{U}$ are respectively the rotation and stretch tensors from the Right Polar Decomposition Theorem and ${}^t_0\boldsymbol{V}$ is the stretch tensor from the Left Polar Decomposition Theorem. The principal stretches $\lambda_i$ $(i = 1, 2, 3)$ are the eigenvalues of both $\boldsymbol{U}$ and $\boldsymbol{V}$. Hyperelastic behavior is obtained from

the existence of a stored energy function $\mathcal{W}$. For the case of isotropy it may be written as (we employ the typical abuse of notation preserving the same symbol for different strain energy functions)

$$\mathcal{W}(\boldsymbol{X}) = \mathcal{W}(\boldsymbol{U}) = \mathcal{W}\left(\boldsymbol{Q}\boldsymbol{U}\boldsymbol{Q}^T\right) = \mathcal{W}(\lambda_1, \lambda_2, \lambda_3) \tag{8}$$

where $\boldsymbol{Q}$ is any rotation tensor. For the isotropic case, the Valanis-Landel hypothesis states that $\mathcal{W}(\lambda_1, \lambda_2, \lambda_3)$ can be written as a sum of three independent, but equal in form, functions $\omega(\lambda_i)$:

$$\mathcal{W}(\boldsymbol{U}) = \mathcal{W}(\lambda_1, \lambda_2, \lambda_3) = \sum_{i=1}^{3} \omega(\lambda_i) = \omega(\lambda_1) + \omega(\lambda_2) + \omega(\lambda_3) \tag{9}$$

An equivalent form in terms of principal logarithmic stretches $E_i = \ln \lambda_i$ may be used

$$\mathcal{W}(\boldsymbol{E}) = \mathcal{W}(E_1, E_2, E_3) = \sum_{i=1}^{3} \omega(E_i) = \omega(E_1) + \omega(E_2) + \omega(E_3) \tag{10}$$

where $\boldsymbol{E} = \ln \boldsymbol{U}$ is the logarithmic strain tensor in the reference configuration.

In the case of transversely isotropic materials, there exist a material preferred direction $\boldsymbol{a}_0$ and an isotropic plane perpendicular to $\boldsymbol{a}_0$. Denoting by $\boldsymbol{Q}_{\boldsymbol{a}_0}$ any rotation with $\boldsymbol{a}_0$ being the real normalized eigenvector, we still obtain $\mathcal{W}(\boldsymbol{U}) = \mathcal{W}(\boldsymbol{Q}_{\boldsymbol{a}_0}\boldsymbol{U}\boldsymbol{Q}_{\boldsymbol{a}_0}^T)$ or, equivalently, $\mathcal{W}(\boldsymbol{E}) = \mathcal{W}(\boldsymbol{Q}_{\boldsymbol{a}_0}\boldsymbol{E}\boldsymbol{Q}_{\boldsymbol{a}_0}^T)$. However, if $\boldsymbol{a}_0$ is not the axis of rotation, in general $\mathcal{W}(\boldsymbol{U}) \neq \mathcal{W}\left(\boldsymbol{Q}\boldsymbol{U}\boldsymbol{Q}^T\right)$

and $\mathcal{W}(\boldsymbol{E}) \neq \mathcal{W}\left(\boldsymbol{Q}\boldsymbol{E}\boldsymbol{Q}^T\right)$. In this case, the strain energy function should be expressed as

$$\mathcal{W}(\boldsymbol{E}, \boldsymbol{a}_0 \otimes \boldsymbol{a}_0) = \mathcal{W}\left(\boldsymbol{Q}\boldsymbol{E}\boldsymbol{Q}^T, \boldsymbol{Q}\boldsymbol{a}_0 \otimes \boldsymbol{a}_0\boldsymbol{Q}^T\right) \tag{11}$$

for any orthogonal tensor $\boldsymbol{Q}$.

Let $\boldsymbol{X}'=\{\boldsymbol{e}'_1, \boldsymbol{e}'_2, \boldsymbol{e}'_3 = \boldsymbol{a}_0\}$ be a Cartesian system of representation in which the third direction is the preferred direction. Then, the logarithmic strain components are

$$\begin{cases} E'_3 = \boldsymbol{a}_0 \cdot \boldsymbol{E} \cdot \boldsymbol{a}_0 = \boldsymbol{E} : (\boldsymbol{a}_0 \otimes \boldsymbol{a}_0) \\ E'_{\alpha\beta} = \boldsymbol{e}'_\alpha \cdot \boldsymbol{E} \cdot \boldsymbol{e}'_\beta = \boldsymbol{E} : \left(\boldsymbol{e}'_\alpha \otimes \boldsymbol{e}'_\beta\right) \\ E'_{\alpha 3} = E'_{3\alpha} = \boldsymbol{e}'_\alpha \cdot \boldsymbol{E} \cdot \boldsymbol{a}_0 = \boldsymbol{E} : (\boldsymbol{e}'_\alpha \otimes \boldsymbol{a}_0) \end{cases} \tag{12}$$

where $\alpha, \beta = 1, 2$ and the symbols $(\cdot)$, $(:)$ and $(\otimes)$ are the one index contraction, the two indices contraction and the dyadic product. In particular, one can choose a reference frame $\boldsymbol{X}_{pr} = \{\boldsymbol{e}_1, \boldsymbol{e}_2, \boldsymbol{e}_3 = \boldsymbol{a}_0\}$ for which $E_{12} = 0$. In this last system of representation, the strain energy function may be expressed as

$$\mathcal{W}(\boldsymbol{E}, \boldsymbol{a}_0 \otimes \boldsymbol{a}_0) = \mathcal{W}(E_1, E_2, E_3, E_{13}, E_{23}) \tag{13}$$

which is a valid function dependency fulfilling the invariance relation (11). We now extend the Valanis-Landel expression to transversely isotropic ma-

terials as

$$\mathcal{W} = \omega_1\left(E_1\right) + \omega_1\left(E_2\right) + \omega_3\left(E_3\right) + 2\omega_{13}\left(\frac{E_{13}+E_{31}}{2}\right) + 2\omega_{13}\left(\frac{E_{23}+E_{32}}{2}\right) \tag{14}$$

where $\omega_1$, $\omega_3$, $\omega_{13}$ are three different, nonsimilar, functions. The arguments of the two terms $\omega_{13}$ accounts for the minor symmetries of the fourth-order elasticity tensor $\partial^2\mathcal{W}/\boldsymbol{\partial E \partial E}$. The factor of 2 is used for convenience, as seen below.

We want to note that the stored energy function given in Eq. (14) provides exact results in any deformation state for incompressible transversely isotropic materials with linear constitutive relations between logarithmic stress and strain measures, $\mathcal{W}$ being in this particular case a quadratic function of each deviatoric strain component, as it occurs in the small strains framework as well. For the nonlinear case, as shown below, decomposition given in Eq. (14) still allows for an exact match of the given experimental data in the material preferred directions, which is the main advantage of this model. However, evidently, for a general deformation state Eq. (14) predicts an hypothetical nonproportional behavior that, up to date and to the authors' knowledge, cannot be verified with the published experiments. Of course, any existing constitutive model which use an explicit form of the strain energy function for transversely isotropic or orthotropic hyperelasticity contains, implicitly, other hypotheses on the coupling of strain components. The accuracy of all those assumptions could be checked only through exten-

sive experimental testing.

Regarding material stability, it is clear that this property is guaranteed if every function in expression (14) is convex. This condition will be easily verified once the piecewise spline representations which define the strain energy function are calculated. Nevertheless, as a result of the presented uncoupled decomposition and the inversion formula, stable stored energy functions will be obtained for stable transversely isotropic materials in most practical cases. Also note that, due to the exact fitting of the experimental data, the model offers the possibility to reproduce real behaviors of unstable materials. Obviously, this type of materials cannot be modelled with other typical hyperelastic models found in the literature that prescribe a stable free energy function by construction.

### *2.3. Stress tensors from hyperelasticity*

The rate of change of the stored energy function, to be equilibrated with the stress power in an elastic process is

$$\mathcal{P} = \dot{\mathcal{W}} = \boldsymbol{S} : \dot{\boldsymbol{A}} = \boldsymbol{T} : \dot{\boldsymbol{E}} \tag{15}$$

where $\boldsymbol{A}$ is the Green-Lagrange strain tensor, $\boldsymbol{S} = \partial\mathcal{W}/\partial\boldsymbol{A}$ is the Second Piola Kirchhoff stress tensor and $\boldsymbol{T} = \partial\mathcal{W}/\partial\boldsymbol{E}$ is the Generalized Kirchhoff stress tensor [19][20]. We have assumed that the preferred direction $\boldsymbol{a}_0$ remains constant in the material configuration. Otherwise, some extra terms need to be added [19][20].

In general, the Generalized Kirchhoff stress tensor does not coincide with the rotated Kirchhoff stress tensor $\bar{\boldsymbol{\tau}}$, except in the case of isotropy, where stresses and strains commute. However, if the principal directions of deformation are the preferred material directions in orthotropy (and hence, in transverse isotropy), then stresses and strains have the same eigenvectors and hence both $\boldsymbol{T}$ and $\bar{\boldsymbol{\tau}}$ are coincident in these particular load cases. Furthermore, for the case of incompressible materials, since the Jacobian determinant $J = \lambda_1\lambda_2\lambda_3 = 1$, $\boldsymbol{T}$ is also coincident with the rotated Cauchy stress tensor $\bar{\boldsymbol{\sigma}}$.

As seen below, for these particular cases of $\boldsymbol{a}_0$ being an eigenvector of the material deformation measures and of incompressible material behavior, we obtain

$$\bar{\boldsymbol{\sigma}} = \boldsymbol{T} = \frac{\partial \mathcal{W}}{\partial \boldsymbol{E}} + p\boldsymbol{I} \tag{16}$$

with $p$ representing a pressure-like quantity (hydrostatic pressure) required to maintain incompressibility, which must be calculated by means of equilibrium requirements and boundary conditions fulfillments. In view of decomposition (14), this last expression lets us perform a stress calculation in the reference system $\boldsymbol{X}_{pr}$ in a very simple way:

$$\bar{\sigma}_1 = \frac{d\omega_1\left(E_1\right)}{dE_1} + p; \qquad \bar{\sigma}_2 = \frac{d\omega_1\left(E_2\right)}{dE_2} + p; \qquad \bar{\sigma}_3 = \frac{d\omega_3\left(E_3\right)}{dE_3} + p \tag{17}$$

For the general case, we note that there exist a mapping between any two strain measures and hence, between their work-conjugate stress measures. A

simple use of the chain rule gives

$$\dot{\boldsymbol{A}} = \frac{\partial \boldsymbol{A}}{\partial \boldsymbol{E}} : \dot{\boldsymbol{E}} \tag{18}$$

where $\partial \boldsymbol{A}/\partial \boldsymbol{E}$ is a fourth order mapping tensor such that

$$\dot{\mathcal{W}} = \boldsymbol{S} : \dot{\boldsymbol{A}} = \boldsymbol{S} : \frac{\partial \boldsymbol{A}}{\partial \boldsymbol{E}} : \dot{\boldsymbol{E}} = \boldsymbol{T} : \dot{\boldsymbol{E}} \;\Rightarrow\; \boldsymbol{T} = \boldsymbol{S} : \frac{\partial \boldsymbol{A}}{\partial \boldsymbol{E}} \tag{19}$$

with

$$\mathbb{M}_{\dot{\boldsymbol{E}}}^{\dot{\boldsymbol{A}}} := \frac{\partial \boldsymbol{A}}{\partial \boldsymbol{E}} = \sum_{i=1}^{3} \lambda_i^2 \boldsymbol{M}_i \otimes \boldsymbol{M}_i + \sum_{i=1}^{3} \sum_{j \neq i} \frac{1}{2} \frac{\lambda_j^2 - \lambda_i^2}{\ln \lambda_j - \ln \lambda_i} \boldsymbol{M}_i \overset{s}{\odot} \boldsymbol{M}_j \tag{20}$$

where $\lambda_i$ are the principal stretches, $\boldsymbol{N}_i$ are the principal directions of $\boldsymbol{U}$ and $\boldsymbol{E}$, and

$$\boldsymbol{M}_i = \boldsymbol{N}_i \otimes \boldsymbol{N}_i \tag{21}$$

$$\boldsymbol{M}_i \overset{s}{\odot} \boldsymbol{M}_j = \frac{1}{4} \left( \boldsymbol{N}_i \otimes \boldsymbol{N}_j + \boldsymbol{N}_j \otimes \boldsymbol{N}_i \right) \otimes \left( \boldsymbol{N}_i \otimes \boldsymbol{N}_j + \boldsymbol{N}_j \otimes \boldsymbol{N}_i \right) \tag{22}$$

Furthermore, if $\boldsymbol{v}$ is the velocity and $\nabla \boldsymbol{v}$ is its spatial gradient, the deformation rate tensor is

$$\begin{aligned} \boldsymbol{d} &= sym\left(\nabla \boldsymbol{v}\right) = \dot{\boldsymbol{X}} \boldsymbol{X}^{-1} + \boldsymbol{X}^{-T} \dot{\boldsymbol{X}}^{T} = \boldsymbol{X}^{-T} \dot{\boldsymbol{A}} \boldsymbol{X}^{-1} \\ &= \boldsymbol{R} \underbrace{\boldsymbol{U}^{-1} \dot{\boldsymbol{A}} \boldsymbol{U}^{-1}}_{\bar{\boldsymbol{d}}} \boldsymbol{R}^{T} = \boldsymbol{R} \left[ \left( \boldsymbol{U}^{-1} \odot \boldsymbol{U}^{-1} \right) : \dot{\boldsymbol{A}} \right] \boldsymbol{R}^{T} \end{aligned} \tag{23}$$

where $\left[\left(\boldsymbol{U}^{-1}\odot\boldsymbol{U}^{-1}\right):\dot{\boldsymbol{A}}\right]_{ij}=U_{ik}^{-1}U_{jl}^{-1}\dot{A}_{kl}$, $\boldsymbol{\tau}$ is the (spatial) Kirchhoff stress tensor and the Stress Power is

$$\mathcal{P}=\boldsymbol{\tau}:\boldsymbol{d}=\bar{\boldsymbol{\tau}}:\bar{\boldsymbol{d}}=\bar{\boldsymbol{\tau}}:\left[\left(\boldsymbol{U}^{-1}\odot\boldsymbol{U}^{-1}\right):\frac{\partial\boldsymbol{A}}{\partial\boldsymbol{E}}:\dot{\boldsymbol{E}}\right]=\underbrace{\bar{\boldsymbol{\tau}}:\mathbb{M}_{\dot{\boldsymbol{E}}}^{\bar{\boldsymbol{d}}}}_{\boldsymbol{T}}:\dot{\boldsymbol{E}} \tag{24}$$

where $\overline{(\cdot)}=\boldsymbol{R}^{T}(\cdot)\boldsymbol{R}$ are the rotated measures and $\boldsymbol{U}^{-1}=\sum_{i=1}^{3}\lambda_i^{-1}\boldsymbol{N}_i\otimes\boldsymbol{N}_i$
The tensor $\mathbb{M}_{\dot{\boldsymbol{E}}}^{\bar{\boldsymbol{d}}}$ is

$$\mathbb{M}_{\dot{\boldsymbol{E}}}^{\bar{\boldsymbol{d}}}:=\left(\boldsymbol{U}^{-1}\odot\boldsymbol{U}^{-1}\right):\frac{\partial\boldsymbol{A}}{\partial\boldsymbol{E}}=\sum_{i=1}^{3}\boldsymbol{M}_i\otimes\boldsymbol{M}_i+\sum_{i=1}^{3}\sum_{j\neq i}\frac{1}{2}\frac{\left(\lambda_j^2-\lambda_i^2\right)/\left(\lambda_i\lambda_j\right)}{\ln\lambda_j-\ln\lambda_i}\boldsymbol{M}_i\overset{s}{\odot}\boldsymbol{M}_j \tag{25}$$

where

$$\lim_{\lambda_i\to\lambda_j}\frac{1}{2}\frac{\left(\lambda_j^2-\lambda_i^2\right)/\left(\lambda_i\lambda_j\right)}{\ln\lambda_j-\ln\lambda_i}=1 \tag{26}$$

Of course both $\boldsymbol{T}$ and $\bar{\boldsymbol{\tau}}$ can be written in the basis of principal stretches

$$\boldsymbol{T}=T_{ij}\boldsymbol{N}_i\otimes\boldsymbol{N}_j;\quad\bar{\boldsymbol{\tau}}=\bar{\tau}_{ij}\boldsymbol{N}_i\otimes\boldsymbol{N}_j \tag{27}$$

and

$$T_{ij}=\frac{1}{2}\frac{\left(\lambda_j^2-\lambda_i^2\right)/\left(\lambda_i\lambda_j\right)}{\ln\lambda_j-\ln\lambda_i}\bar{\tau}_{ij} \tag{28}$$

where in general $T_{ij}\neq 0$ for $i\neq j$ due to the lack of isotropy ($\bar{\tau}_{ij}\neq 0$). Thus, the diagonal terms of both $\boldsymbol{T}$ and $\bar{\boldsymbol{\tau}}$ are coincident (and if $J=1$ also coincident to the rotated Cauchy stress tensor), whereas the shear terms

differ slightly. In the case of simple shear

$$T_{ij} = \frac{1}{4}\frac{(\lambda^2 - 1/\lambda^2)}{\ln \lambda}\bar{\tau}_{ij} \tag{29}$$

where $\lambda$ and $1/\lambda$ are the two principal stretches, see Section 3.2.2.

*2.4. The inversion formula*

Consider the following relation, which generalizes the one given in Reference [17]

$$f(x) = g(x) - g(y(x)) \tag{30}$$

where $f(x)$ and $y(x)$ are known functions and $g(x)$ is the unknown, being all of them continuous functions in all the domain of interest. Let $y^{(K)}(x)$ be the *K-th* composition of function $y(x)$, that is

$$y^{(0)}(x) = x \tag{31}$$

$$y^{(1)}(x) = y(x) \tag{32}$$

$$y^{(2)}(x) = y(y(x)) \tag{33}$$

$$\vdots$$

$$y^{(K)}(x) = \underbrace{y(y(...(y}_{K}(x))...)) \tag{34}$$

Then, evidently

$$f(x) = g(x) - g(y(x)) \tag{35}$$

$$f(y(x)) = g(y(x)) - g\left(y^{(2)}(x)\right) \tag{36}$$

$$f\left(y^{(2)}(x)\right) = g\left(y^{(2)}(x)\right) - g\left(y^{(3)}(x)\right) \tag{37}$$

$$\vdots$$

$$f\left(y^{(K)}(x)\right) = g\left(y^{(K)}(x)\right) - g\left(y^{(K+1)}(x)\right) \tag{38}$$

Summing both sides of this set of equations gives

$$\sum_{k=0}^{K} f\left(y^{(k)}(x)\right) = g(x) - g\left(y^{(K+1)}(x)\right) \tag{39}$$

When the assumptions $|y(x)| < |x|$ and $g(0) = 0$ are introduced, then $\lim_{K\to\infty} g\left(y^{(K)}(x)\right) = g(0) = 0$ and Eq. (39) yields

$$g(x) = \sum_{k=0}^{\infty} f\left(y^{(k)}(x)\right) \tag{40}$$

for $K \to \infty$, which provides an exact solution of Eq. (30). Also, note that for $x = 0$, Eq. (40) provides the result $f(0) = 0$, which is another assumption to be regarded.

## 3. Strain-energy function determination from experimental data

There are several cases, depending on the available test data, in which the stored-energy function (14) may be determined using the concepts and formulations developed in the previous section. In each case, only the test data used to obtain $\mathcal{W}(\boldsymbol{E}, \boldsymbol{a}_0)$ will be reproduced almost exactly with the spline model, obtaining an approximation for the remaining stresses. Hence, if there are available test data that make it possible to follow more than one procedure, the user should select the procedure that better fits the problem at hand.

Next, throughout Sections 3.1.1–3.1.3 we illustrate the methodology we follow to obtain the first derivative of the unknown functions $\omega_1$ and $\omega_3$ in each one of the three possible cases we consider. The procedures to calculate $\omega'_{13}$ will be presented subsequently, in Sections 3.2.1 and 3.2.2.

### *3.1. Determination of $\omega_1$ and $\omega_3$*

#### *3.1.1. One uniaxial test in a (transversely) isotropic direction*

It is not the most common case to have only this type of experimental data or to consider it as the most important set. However, we start with this case because it is the simplest one to analyze. Since this uniaxial test is carried out along one of the preferred material axes of $\boldsymbol{X}_{pr}$, we will be able to refer indistinctly to $\boldsymbol{\sigma}$, $\bar{\boldsymbol{\sigma}}$, $\bar{\boldsymbol{\tau}}$ or $\boldsymbol{T}$.

The initial measured data points are $(\widetilde{E}_1, \widetilde{\sigma}_1)$ and $(\widetilde{E}_1, \widetilde{E}_2)$, where the subscripts indicate the corresponding directions of the reference system $\boldsymbol{X}_{pr}$ and

the tilde decoration has been used to indicate the experimental and discrete nature of these data points. We will refer to that initial data points as $\widetilde{\sigma}_1(\widetilde{E}_1)$ and $\widetilde{E}_2(\widetilde{E}_1)$, where the quantity in parenthesis specifies the type of test, i.e. $\widetilde{\sigma}_1(\widetilde{E}_1) \Leftrightarrow (\widetilde{E}_1, \widetilde{\sigma}_1)$. Thus, $\widetilde{\sigma}_1(\widetilde{E}_1)$ represents the normal Cauchy stress in the isotropic direction being tested ($\boldsymbol{e}_1$) as a discrete function of the longitudinal logarithmic strain in that direction, for tension and compression. Data $\widetilde{E}_2(\widetilde{E}_1)$ represent the Hencky strain in the transversely isotropic direction $\boldsymbol{e}_2$, also as a discrete function of $\widetilde{E}_1$. In this case the function $\mathcal{W}(\boldsymbol{E}, \boldsymbol{a}_0)$ to be obtained is able to closely (or exactly) predict the experimental points $\widetilde{\sigma}_1(\widetilde{E}_1)$.

From the known data $\widetilde{\sigma}_1(\widetilde{E}_1)$ and $\widetilde{E}_2(\widetilde{E}_1)$, according to (17) the following relations hold:

$$\begin{cases} \widetilde{\sigma}_1(\widetilde{E}_1) = \left.\dfrac{d\omega_1(E_1)}{dE_1}\right|_{\widetilde{E}_1} + p \\ \\ 0 = \left.\dfrac{d\omega_1(E_2)}{dE_2}\right|_{\widetilde{E}_2(\widetilde{E}_1)} + p \\ \\ 0 = \left.\dfrac{d\omega_3(E_3)}{dE_3}\right|_{\widetilde{E}_3(\widetilde{E}_1)} + p \end{cases} \tag{41}$$

where the normal Cauchy stresses in both transversal directions ($\boldsymbol{e}_2$ and $\boldsymbol{e}_3$) have been made equal to zero and the transversal strain in direction $\boldsymbol{e}_3$ is

$$\widetilde{E}_3(\widetilde{E}_1) = -\widetilde{E}_1 - \widetilde{E}_2(\widetilde{E}_1) \tag{42}$$

which is a known discrete function of $\widetilde{E}_1$ obtained from the incompressibility constraint $\widetilde{E}_1 + \widetilde{E}_2(\widetilde{E}_1) + \widetilde{E}_3(\widetilde{E}_1) = 0$. Thus, factoring out the pressure from the second equation of (41) and inserting the result in the first and third equations, we obtain

$$\widetilde{\sigma}_1(\widetilde{E}_1) = \left.\frac{d\omega_1(E_1)}{dE_1}\right|_{\widetilde{E}_1} - \left.\frac{d\omega_1(E_2)}{dE_2}\right|_{\widetilde{E}_2(\widetilde{E}_1)} \tag{43}$$

$$\left.\frac{d\omega_1(E_2)}{dE_2}\right|_{\widetilde{E}_2(\widetilde{E}_1)} = \left.\frac{d\omega_3(E_3)}{dE_3}\right|_{\widetilde{E}_3(\widetilde{E}_1)} \tag{44}$$

From Equation (43) it is possible to determine the first derivative function $\omega_1'(E_1)$. Then, Equation (44), which may be interpreted as a compatibility condition involving the derivative functions $\omega_1'$ and $\omega_3'$, provides the calculation of the other unknown function $\omega_3'(E_3)$. If the experimental transverse strains in the anisotropic direction $\widetilde{E}_3(\widetilde{E}_1)$ were available instead of $\widetilde{E}_2(\widetilde{E}_1)$, the initially unknown distribution $\widetilde{E}_2(\widetilde{E}_1)$ could be directly obtained from the incompressibility condition and the procedure detailed next could be applied in the same manner. The procedure using splines (Section 2.1) and the inversion formula (Section 2.4) is as follows.

First, the measured data points $\widetilde{\sigma}_1(\widetilde{E}_1)$ and $\widetilde{E}_2(\widetilde{E}_1)$ are interpolated using non-uniform piecewise cubic splines, as shown in Figure 1. In that figure, a set of assumed "experimental" data points $\widetilde{\sigma}_1(\widetilde{E}_1)$ and $\widetilde{E}_2(\widetilde{E}_1)$ are presented. We note that the specific values of stresses and strains are irrelevant for the purpose of this section. Actual experimental values are given in Section 4.

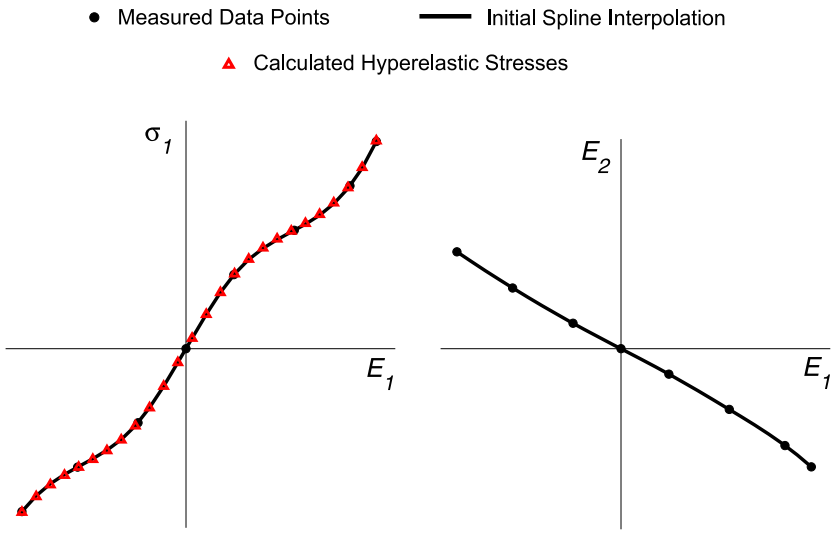


Figure 1: Assumed "measured"data points $\widetilde{\sigma}_1(\widetilde{E}_1)$ and $\widetilde{E}_2(\widetilde{E}_1)$, their initial non-uniform piecewise spline interpolations $\sigma_1(E_1)$ and $E_2(E_1)$ and calculated stresses $\overline{\sigma}_1(\overline{E}_1)$ using Eq. (48) (or Eq. (49)) with the corresponding spline-based energy functions (see Fig. 2).

We denote by $\sigma_1(E_1)$ and $E_2(E_1)$ –solid lines– the piecewise spline functions interpolating the data points $\widetilde{\sigma}_1(\widetilde{E}_1)$ and $\widetilde{E}_2(\widetilde{E}_1)$ –solid circles–, respectively.

For increasing numerical efficiency during the finite element analysis, uniform intervals are preferred, because then the specific interval for a given value of strain can be easily determined. Therefore, the domain $[\widetilde{E}_{1min}, \widetilde{E}_{1max}]$ is divided into $N_1$ uniform intervals with equally-spaced points $\overline{E}_1$. Using these new $N_1+1$ points $\overline{E}_1$ and their corresponding values $\sigma_1(\overline{E}_1)$ and $E_2(\overline{E}_1)$, obtained from the spline functions $\sigma_1(E_1)$ and $E_2(E_1)$ respectively, Eqs. (43) and (44) can be rewritten in the following way

$$\sigma_1(\overline{E}_1) = \omega_1'(\overline{E}_1) - \omega_1'\left(E_2(\overline{E}_1)\right) \tag{45}$$

$$\omega_1'\left(E_2(\overline{E}_1)\right) = \omega_3'\left(E_3(\overline{E}_1)\right) \tag{46}$$

where $E_3(E_1)$ represents the piecewise spline function that interpolates the data points $\left(\overline{E}_1, E_3\left(\overline{E}_1\right)\right) = \left(\overline{E}_1, -\overline{E}_1 - \overline{E}_2\right)$. Note that Equation (45) adopts the form of Equation (30). Hence, provided that $\sigma_1(0) = 0$ (the reference configuration is stress-free) and $|E_2(E_1)| < |E_1|$, since it can also be assumed that $\omega_1'(0) = 0$, the solution (40) can be applied to calculate each value $\omega_1'(\overline{E}_1)$ in Eq. (45) through

$$\omega_1'(\overline{E}_1) = \sum_{k=0}^{K} \sigma_1(E_2^{(k)}(\overline{E}_1)) \tag{47}$$

In Eq. (47) the spline functions $E_2(E_1)$ and $\sigma_1(E_1)$ make possible the evaluation of all the terms in the summation. Note also that this last expression is more compact than the one provided in Reference [17]. In practical anisotropic cases, $-E_1 < E_2(E_1) < 0$ (for isotropic materials, $E_2(E_1) = -E_1/2$) so Eq. (47) can effectively be applied to solve Eq. (45). In practice, the number of terms to consider is chosen so that the contribution of the *K-th* term to the sum is negligible (smaller than a given tolerance), that is, when $\sigma_1(E_2^{(K)}(\overline{E}_1)) \ll \sigma_1(E_2^{(0)}(\overline{E}_1)) = \sigma_1(\overline{E}_1)$. Once all the $N+1$ values $\omega_1'(\overline{E}_1)$ are calculated using Equation (47), the corresponding piecewise spline function $\omega_1'(E_1)$ can be constructed. Subsequently, the calculated function $\omega_1'(E_1)$ evaluated at points $E_2(\overline{E}_1)$, together with Eq. (46), let us obtain all the values $\omega_3'\left(E_3(\overline{E}_1)\right)$. Then, as before, the piecewise spline representation $\omega_3'(E_3)$ can be constructed, as shown in Figure 2, where the spline

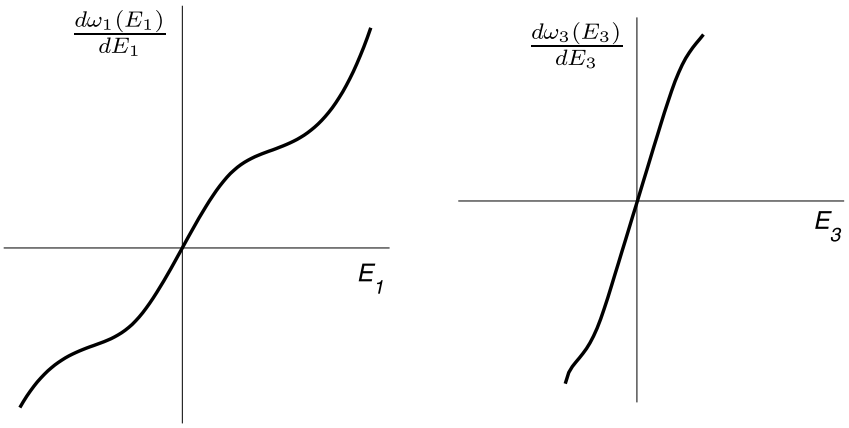


Figure 2: Uniform piecewise spline representations $\omega_1'(E_1)$ and $\omega_3'(E_3)$ obtained from "measured" data points represented in Fig. 1. The splines have been built from the previously calculated values $\omega_1'(\overline{E}_1)$ using Eq. (47) and $\omega_3'(E_3(\overline{E}_1))$ using Relation (46).

function $\omega_1'(E_1)$ has also been depicted.

These piecewise cubic spline representations, i.e. $\omega_1'(E_1)$ and $\omega_3'(E_3)$, described by their respective spline coefficients (Section 2.1), are the functions to be implemented in the finite element code. Although these functions can not be expressed in a compact analytical form, like Ogden's or other hyperelastic models, note that they are piecewise analytical functions with first and second derivatives being continuous in all their respective domains. This implies that the strain-energy function given in Eq. (14) has continuous derivatives until third order, which is an interesting property for equilibrium iterations.

In Figure 1 the stress points $\overline{\sigma}_1(\overline{E}_1)$ obtained from the energy functions

$\omega_1'(E_1)$ and $\omega_3'(E_3)$, that is

$$\overline{\sigma}_1(\overline{E}_1) = \omega_1'(\overline{E}_1) - \omega_1'\left(E_2(\overline{E}_1)\right) \tag{48}$$

$$= \omega_1'(\overline{E}_1) - \omega_3'\left(E_3(\overline{E}_1)\right) \tag{49}$$

are also represented. It can be seen that the calculated distribution $\overline{\sigma}_1(\overline{E}_1)$ reproduces exactly the original spline function $\sigma_1(E_1)$.

For convenience, the overall procedure is summarized in Table 1.

**Calculation of $\omega_1'(E_1)$ and $\omega_3'(E_3)$**

1. Experimental data: $\widetilde{\sigma}_1(\widetilde{E}_1)$ and $\widetilde{E}_2(\widetilde{E}_1)$ from a tension-compression uniaxial test.
2. Build (non-uniform) piecewise spline functions: $\sigma_1(E_1)$ from $\widetilde{\sigma}_1(\widetilde{E}_1)$ and $E_2(E_1)$ from$\widetilde{E}_2(\widetilde{E}_1)$.
3. Divide the domain $[\widetilde{E}_{1min}, \widetilde{E}_{1max}]$ into $N_1$ uniform intervals with $N_1 + 1$ equally spaced points $\overline{E}_1$.
4. Build the spline representation $E_3(E_1)$ from points $\left(\overline{E}_1, E_3\left(\overline{E}_1\right)\right) = \left(\overline{E}_1, -\overline{E}_1 - \overline{E}_2\right)$.
5. For each strain measure $\overline{E}_1$, calculate $\omega_1'(\overline{E}_1)$ with Eq.(47).
6. With values $\omega_1'(\overline{E}_1)$ compute the uniform spline function $\omega_1'(E_1)$.
7. With $\omega_1'(E_1)$ evaluated at points $E_2(\overline{E}_1)$, compute $\omega_3'\left(E_3(\overline{E}_1)\right)$ using Eq.(46) and the spline function $E_3(E_1)$.
8. Form piecewise spline $\omega_3'(E_3)$ from all the values $\omega_3'\left(E_3(\overline{E}_1)\right)$ obtained in the previous step.

Table 1: Computational procedure for the case of Section 3.1.1

We finally note that if the compression interval $[\widetilde{E}_{1min}, 0]$ is rather smaller than the tension range $[0, \widetilde{E}_{1max}]$, then the value $E_2(\widetilde{E}_{1max})$ may not be within the interval $[\widetilde{E}_{1min}, 0]$ and $\omega_1'(\widetilde{E}_{1max})$ could not be calculated using the spline function $\sigma_1(E_1)$ in Eq. (47) at Step 5 of Table 1. In these

cases, the domain $[\widetilde{E}_{1min}, \widetilde{E}_{1max}]$ has to be extended to a new larger domain $[\widetilde{E}^*_{1min}, \widetilde{E}_{1max}] = [E_2(\widetilde{E}_{1max}), \widetilde{E}_{1max}]$, being necessary to extrapolate the spline functions $\sigma_1(E_1)$ and $E_2(E_1)$ until the new lower limit $\widetilde{E}^*_{1min}$. The case in which $\widetilde{E}_{1max} < E_2(\widetilde{E}_{1min})$ is circumvented in an analogous way. These issues should be checked before starting the procedure detailed in Table 1. However, we do not include these checks in the table for simplicity.

### *3.1.2. Two independent uniaxial tests in isotropic and anisotropic directions (case A)*

For the case in which two uniaxial tests have been performed separately over the material under study, we show two possibilities to obtain the strain-energy function given in Eq. (14) depending on the available test data.

For the procedure illustrated herein, the initial measured data points are $(\widetilde{E}_3, \widetilde{\sigma}_3)$ from the tension-compression test performed in the preferred direction $\boldsymbol{e}_3$ and $(\widetilde{E}_1, \widetilde{E}_2)$ from the uniaxial test along direction $\boldsymbol{e}_1$. We will denote those measured data points as $\widetilde{\sigma}_3(\widetilde{E}_3)$ and $\widetilde{E}_2(\widetilde{E}_1)$. In this case, the function $\mathcal{W}(\boldsymbol{E}, \boldsymbol{a}_0)$ to be obtained is able to predict very accurately the stress distribution $\widetilde{\sigma}_3(\widetilde{E}_3)$.

From the experimental points $\widetilde{\sigma}_3(\widetilde{E}_3)$, according to Eq.(17) we can write

$$\begin{cases} \widetilde{\sigma}_3(\widetilde{E}_3) = \left.\dfrac{d\omega_3\left(E_3\right)}{dE_3}\right|_{\widetilde{E}_3} + p \\ \\ 0 = \left.\dfrac{d\omega_1\left(E_1\right)}{dE_1}\right|_{-\widetilde{E}_3/2} + p \\ \\ 0 = \left.\dfrac{d\omega_1\left(E_2\right)}{dE_2}\right|_{-\widetilde{E}_3/2} + p \end{cases} \tag{50}$$

and proceeding as before

$$\widetilde{\sigma}_3(\widetilde{E}_3) = \left.\frac{d\omega_3\left(E_3\right)}{dE_3}\right|_{\widetilde{E}_3} - \left.\frac{d\omega_1\left(E_1\right)}{dE_1}\right|_{-\widetilde{E}_3/2} \tag{51}$$

$$\left.\frac{d\omega_1\left(E_1\right)}{dE_1}\right|_{-\widetilde{E}_3/2} = \left.\frac{d\omega_1\left(E_2\right)}{dE_2}\right|_{-\widetilde{E}_3/2} \tag{52}$$

where, due to the transverse isotropy and the incompressibility constraint, the following relations have been used

$$\widetilde{E}_1(\widetilde{E}_3) = \widetilde{E}_2(\widetilde{E}_3) = -\frac{\widetilde{E}_3}{2} \tag{53}$$

Moreover, note that Equation (52) is now an identity which always holds, so it will be not necessary to consider this equation anymore.

For the other test, only the transverse strains $\widetilde{E}_2(\widetilde{E}_1)$ are known, so only

the transverse equations are considered

$$\begin{cases} 0 = \left.\dfrac{d\omega_1\left(E_2\right)}{dE_2}\right|_{\widetilde{E}_2(\widetilde{E}_1)} + p \\ \\ 0 = \left.\dfrac{d\omega_3\left(E_3\right)}{dE_3}\right|_{\widetilde{E}_3(\widetilde{E}_1)} + p \end{cases} \tag{54}$$

Then, we obtain

$$\left.\frac{d\omega_1\left(E_2\right)}{dE_2}\right|_{\widetilde{E}_2(\widetilde{E}_1)} = \left.\frac{d\omega_3\left(E_3\right)}{dE_3}\right|_{\widetilde{E}_3(\widetilde{E}_1)} \tag{55}$$

where the transversal strains in direction $\boldsymbol{e}_3$, $\widetilde{E}_3(\widetilde{E}_1)$, would be easily calculated from the incompressibility condition $\widetilde{E}_1 + \widetilde{E}_2(\widetilde{E}_1) + \widetilde{E}_3(\widetilde{E}_1) = 0$.

From Equations (51) and (55), we can obtain the first derivative functions $\omega_1'$ and $\omega_3'$ as follows. In the same way as in the previous case, the experimental points $\widetilde{\sigma}_3(\widetilde{E}_3)$ and $\widetilde{E}_2(\widetilde{E}_1)$ are interpolated using non-uniform piecewise cubic splines, i.e. $\sigma_3(E_3)$ and $E_2(E_1)$ respectively, as shown in Figure 3.

Then, the domains $[\widetilde{E}_{3min}, \widetilde{E}_{3max}]$ and $[\widetilde{E}_{1min}, \widetilde{E}_{1max}]$ are divided into $N_3$ and $N_1$ uniform intervals, which define the new $N_3 + 1$ and $N_1 + 1$ points $\overline{E}_3$ and $\overline{E}_1$, respectively. Using the spline functions $\sigma_3(E_3)$ evaluated at points $\overline{E}_3$ and $E_2(E_1)$ evaluated at points $\overline{E}_1$, Equations (51) and (55) can be rewritten in the following way

$$\sigma_3(\overline{E}_3) = \omega_3'(\overline{E}_3) - \omega_1'(-\frac{\overline{E}_3}{2}) \tag{56}$$

$$\omega_1'\left(E_2(\overline{E}_1)\right) = \omega_3'\left(E_3(\overline{E}_1)\right) \tag{57}$$

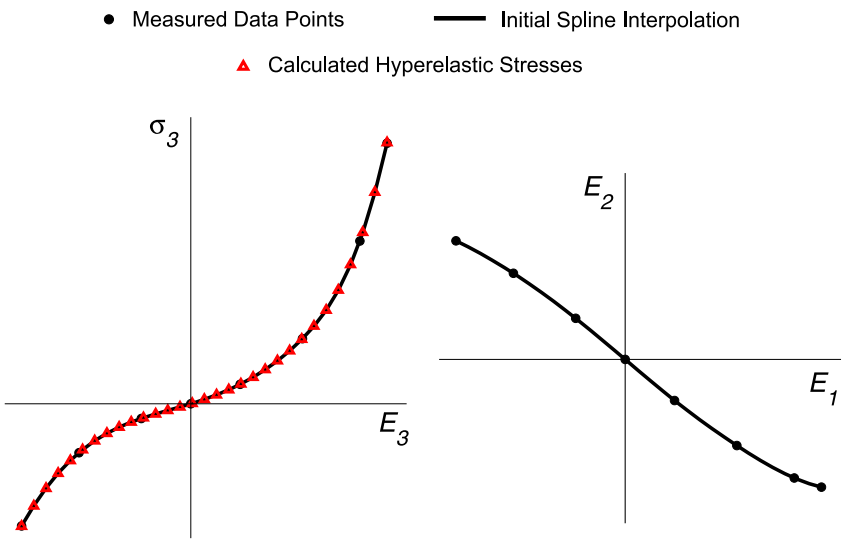


Figure 3: Assumed "measured"data points $\widetilde{\sigma}_3(\widetilde{E}_3)$ from the test in anisotropic direction $\boldsymbol{e}_3$ and $\widetilde{E}_2(\widetilde{E}_1)$ from the test in isotropic direction $\boldsymbol{e}_1$, their initial non-uniform piecewise spline interpolations $\sigma_3(E_3)$ and $E_2(E_1)$ and calculated stresses $\overline{\sigma}_3(\overline{E}_3)$ using Eq. (61) (or Eq. (62)) with the corresponding spline-based energy functions (see Fig. 4).

A crucial difference with respect to the previous case, in which Eq. (45) was solved directly, is that two different functions $\omega_3'$ and $\omega_1'$ are present in Eq. (56), so an inversion such as Eq. (47) can not be performed directly. However, note that Eq. (57) gives a relationship that may be replaced into Eq. (56) to obtain an expression which only depends on function $\omega_3'\left(E_3\right)$ and, therefore, becoming an invertible equation. To do this, it is convenient to eliminate the dependency of $\overline{E}_1$ in Eq. (57) and rewrite it again as

$$\omega_1'(\overline{E}_2) = \omega_3'\left(E_3(\overline{E}_2)\right) \tag{58}$$

where the function $E_3\left(E_2\right)$ represents the piecewise spline function that interpolates the data points $\left(E_2\left(\overline{E}_1\right), E_3\left(\overline{E}_1\right)\right) = \left(\overline{E}_2, -\overline{E}_1 - \overline{E}_2\right)$, all of them corresponding to the test in direction $\boldsymbol{e}_1$. Equation (58) expressed in that way can be replaced into Eq. (56) to give

$$\sigma_3(\overline{E}_3) = \omega_3'(\overline{E}_3) - \omega_3'\left(E_3(-\frac{\overline{E}_3}{2})\right) \tag{59}$$

where $E_3(-\overline{E}_3/2)$ represents the value given by the spline function $E_3\left(E_2\right)$ when $E_2 = -\overline{E}_3/2$. Now, in order to be able to apply the inversion formula given in Eq. (40), we define a new function $E(E_3)$ such that $E(\overline{E}_3) = E_3(-\overline{E}_3/2)$, which will play the role of function $y\left(x\right)$ in Eq.(30). Then, the

$N_3 + 1$ values $\omega_3'(\overline{E}_3)$ can be calculated through

$$\omega_3'(\overline{E}_3) = \sum_{k=0}^{K} \sigma_3(E^{(k)}(\overline{E}_3)) \tag{60}$$

Subsequently, the construction of the corresponding piecewise spline function $\omega_3'(E_3)$ is carried out, which is depicted in Figure 4. As explained above, the mathematical constraint $|E(E_3)| < |E_3|$ must be satisfied so that the summation (60) converges to a finite value for each strain $\overline{E}_3$. It can be shown that the allowed range $-E_3 < E(E_3) < 0$ is equivalent to $-E_1 < E_2(E_1) < -E_1/3$ and that the non-valid values $-\infty < E(E_3) \leq -E_3$ correspond to $-E_1/3 \leq E_2(E_1) < 0$. Hence, only materials with the physical behavior $-E_1 < E_2(E_1) < -E_1/3$ may be dealt with the procedure explained in this section. The values $-E_1 < E_2(E_1) < -E_1/2$ are typical in most practical cases, for which stiffness along the preferred direction $\boldsymbol{e}_3$ is larger than in the transversely isotropic directions. Moreover, materials being moderately less stiff along the preferred direction than in any direction belonging to the orthogonal isotropic plane, i.e. $-E_1/2 < E_2(E_1) < -E_1/3$, may also be studied with this methodology. The summation given in Eq.(60) does not converge for the few (but physically possible) cases $-E_1/3 \leq E_2(E_1) < 0$, although it can be shown that another inversion formula similar to Eq. (60) may be applied for those particular cases.

The spline functions $\omega_3'(E_3)$ and $E_3\,(E_2)$, together with relationship (58), let us obtain the values $\omega_1'(\overline{E}_2)$ and, finally, construct the spline representa-

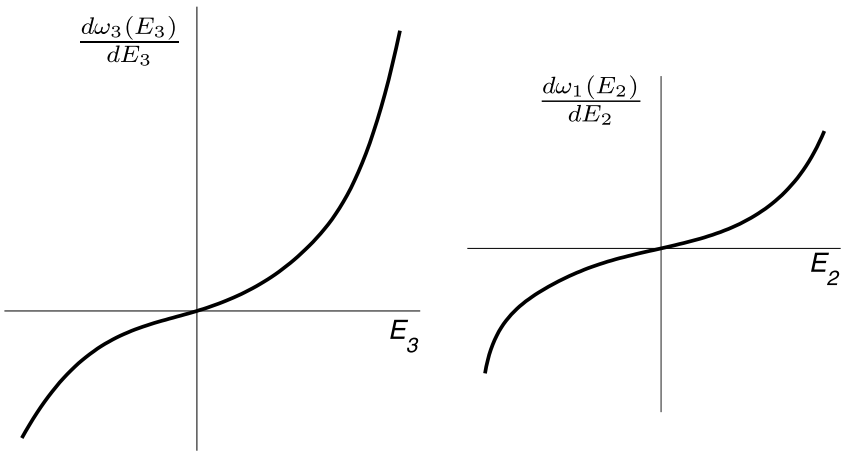


Figure 4: Uniform piecewise spline representations $\omega_3'(E_3)$ and $\omega_1'(E_2)$ corresponding to the data represented in Fig. 3. The splines have been constructed from the previously calculated values $\omega_3'(\overline{E}_3)$ using Eq. (60) and $\omega_1'(\overline{E}_2)$ using Relation (58).

tion $\omega_1'(E_2)$, as shown in Figure 4.

The piecewise spline functions $\omega_3'(E_3)$ and $\omega_1'(E_2)$ may be used to calculate the hyperelastic stress values through

$$\overline{\sigma}_3(\overline{E}_3) = \omega_3'(\overline{E}_3) - \omega_3'\left(E_3(-\frac{\overline{E}_3}{2})\right) \tag{61}$$

$$= \omega_3'(\overline{E}_3) - \omega_1'\left(-\frac{\overline{E}_3}{2}\right) \tag{62}$$

The stress values calculated using Eqs. (61) or (62) are represented in Figure 3, where it can be seen that there exists a perfect agreement with the original test measures.

The overall procedure to obtain the first derivative functions $\omega_3'(E_3)$ and

$\omega_1'(E_2)$ is summarized in Table 2.

**Calculation of $\omega_1'(E_1)$ and $\omega_3'(E_3)$**

1. Experimental data: $\widetilde{\sigma}_3(\widetilde{E}_3)$ and $\widetilde{E}_2(\widetilde{E}_1)$ from tension-compression uniaxial tests.
2. Build (non-uniform) piecewise spline functions: $\sigma_3(E_3)$ from $\widetilde{\sigma}_3(\widetilde{E}_3)$ and $E_2(E_1)$ from $\widetilde{E}_2(\widetilde{E}_1)$.
3. Divide the domains $[\widetilde{E}_{3min}, \widetilde{E}_{3max}]$ and $[\widetilde{E}_{1min}, \widetilde{E}_{1max}]$ into $N_3$ and $N_1$ uniform intervals which define the new $N_3+1$ and $N_1+1$ points $\overline{E}_3$ and $\overline{E}_1$, respectively.
4. Build the spline representation $E_3(E_2)$ from points $\left(E_2\left(\overline{E}_1\right), E_3\left(\overline{E}_1\right)\right) = \left(\overline{E}_2, -\overline{E}_1 - \overline{E}_2\right)$.
5. For each strain measure $\overline{E}_3$, calculate $\omega_3'(\overline{E}_3)$ with Eq.(60) using the composite function $E(\overline{E}_3) = E_3(-\overline{E}_3/2)$.
6. With all the values $\omega_3'(\overline{E}_3)$ compute the uniform spline function $\omega_3'(E_3)$.
7. With $\omega_3'(E_3)$ evaluated at $E_3(\overline{E}_2)$, obtain $\omega_1'\left(\overline{E}_2\right)$ using Eq. (58).
8. Form piecewise spline $\omega_1'(E_2)$ from all the values $\omega_1'\left(\overline{E}_2\right)$ obtained in the previous step.

Table 2: Computational procedure for the case of Section 3.1.2

The same way as in the previous case, in some specific circumstances, the splines used in the procedure detailed in Table 2 must be extrapolated until new lower and upper limits. These checkings should be made before starting with the computations given in the table.

*3.1.3. Two independent uniaxial tests in isotropic and anisotropic directions (case B)*

The case when the available test measures are the tension-compression stress distributions $\widetilde{\sigma}_1(\widetilde{E}_1)$ and $\widetilde{\sigma}_3(\widetilde{E}_3)$ is the most interesting and usual case. The procedure to obtain the functions $\omega_1$ and $\omega_3$ is based on the two previous

cases. The equations to use for the uniaxial test in the isotropic direction $\boldsymbol{e}_1$ are very similar to those applied in Section 3.1.1, namely:

$$\widetilde{\sigma}_1(\widetilde{E}_1) = \left.\frac{d\omega_1\left(E_1\right)}{dE_1}\right|_{\widetilde{E}_1} - \left.\frac{d\omega_1\left(E_2\right)}{dE_2}\right|_{\widetilde{E}_2(\widetilde{E}_1)} \tag{63}$$

$$\left.\frac{d\omega_1\left(E_2\right)}{dE_2}\right|_{\widetilde{E}_2(\widetilde{E}_1)} = \left.\frac{d\omega_3\left(E_3\right)}{dE_3}\right|_{\widetilde{E}_3(\widetilde{E}_1)} \tag{64}$$

where the only difference between Eqs.(43)–(44) and Eqs.(63)–(64) is that in the latter expressions the distributions $\widetilde{E}_2(\widetilde{E}_1)$ and $\widetilde{E}_3(\widetilde{E}_1)$ remain undetermined, whereas in Eqs.(43)–(44) the distributions $\widetilde{E}_2(\widetilde{E}_1)$ and $\widetilde{E}_3(\widetilde{E}_1)$ were known values. However, in this case, these variables are still subjected to the incompressibility condition of the material, i.e., $\widetilde{E}_1 + \widetilde{E}_2(\widetilde{E}_1) + \widetilde{E}_3(\widetilde{E}_1) = 0$.

On the other hand, the transverse strain distributions for the uniaxial test in the preferred direction $\boldsymbol{e}_3$ are known from relations given in Eq.(53), so Eq.(51) also applies in the present context

$$\widetilde{\sigma}_3(\widetilde{E}_3) = \left.\frac{d\omega_3\left(E_3\right)}{dE_3}\right|_{\widetilde{E}_3} - \left.\frac{d\omega_1\left(E_1\right)}{dE_1}\right|_{-\widetilde{E}_3/2} \tag{65}$$

We remind that the other equation for this test, i.e. Eq.(52), always holds. Hence, Eqs.(63), (64) and (65) are the governing equations of this last and more usual case and can be solved as follows.

We first assume a distribution $\widehat{E}_2(\widetilde{E}_1)$ depending on a finite number of (yet unknown) parameters, which will be determined as the final result of the procedure. The hat decoration is used to indicate that the distribution is

assumed. For instance, a linear behavior $\widehat{E}_2(\widetilde{E}_1) = k\widetilde{E}_1$ could be proposed, with only one parameter to be calculated.

Assume now that specific values are given to those parameters. Then, the initial data which define each one of the two previous cases are recovered. On one hand, stresses $\widetilde{\sigma}_1(\widetilde{E}_1)$ and transversal strains $\widehat{E}_2(\widetilde{E}_1)$ are known, so we may calculate the first derivative function $\widehat{\omega}_1'(E_1)$ with the inversion formula and the spline methodology, as indicated in Table 1, steps 1 to 6. On other hand, with $\widetilde{\sigma}_3(\widetilde{E}_3)$ and $\widehat{E}_2(\widetilde{E}_1)$, it is also possible to obtain $\widehat{\omega}_3'(E_3)$ as explained in Table 2, steps 1 to 6. Due to the exact results provided by the inversion formula, measured data points $\widetilde{\sigma}_1(\widetilde{E}_1)$ and $\widetilde{\sigma}_3(\widetilde{E}_3)$ are exactly reproduced by Eqs. (48) and (61) using functions $\widehat{\omega}_1'(E_1)$ and $\widehat{\omega}_3'(E_3)$, respectively. However, since functions $\widehat{\omega}_1'(E_1)$ and $\widehat{\omega}_3'(E_3)$ have been calculated separately, in general, the compatibility relation (64) will not be satisfied and the stresses obtained by means of Eqs.(49) and (62), which involve the evaluation of both functions, will not reproduce the original distributions $\widetilde{\sigma}_1(\widetilde{E}_1)$ and $\widetilde{\sigma}_3(\widetilde{E}_3)$. Hence, the key to solve this case is to find the specific (predefined) distribution $\widehat{E}_2(\widetilde{E}_1)$ which provides the best fulfillment of Equation (64) and which, equivalently, results in the best fit for $\widetilde{\sigma}_1(\widetilde{E}_1)$ and $\widetilde{\sigma}_3(\widetilde{E}_3)$ by means of Eqs.(49) and (62).

Let us define the errors associated to the fulfillment of Eq.(64) as

$$\widehat{err}(\overline{E}_1) = \widehat{\omega}_1'\left(\widehat{E}_2(\overline{E}_1)\right) - \widehat{\omega}_3'\left(\widehat{E}_3(\overline{E}_1)\right) \tag{66}$$

which is calculated for the $N_1 + 1$ strain values $\overline{E}_1$. With this error distribution, the least-squares method can be applied with the following objective function

$$\widehat{S} = \sum_{i=1}^{N_1+1} \left( \widehat{err}(\overline{E}_1^{(i)}) \right)^2 \tag{67}$$

The distribution $\widehat{E}_2(\widetilde{E}_1)$ which minimizes (67) provides the (approximated) solution of the governing Equations (63), (64) and (65).

A step-by-step implementation of the overall algorithmic procedure is given in Table 3. We show the application of this procedure in two examples below.

**Calculation of $\omega_1'(E_1)$ and $\omega_3'(E_3)$**

1. Experimental data: $\widetilde{\sigma}_1(\widetilde{E}_1)$ and $\widetilde{\sigma}_3(\widetilde{E}_3)$ from tension-compression uniaxial tests.
2. Propose a distribution $\widehat{E}_2(\widetilde{E}_1)$ depending on several parameters that you freely specify.
3. With $\widetilde{\sigma}_1(\widetilde{E}_1)$ and $\widehat{E}_2(\widetilde{E}_1)$, follow Steps 1 to 6 of Table 1 to obtain the uniform spline function $\widehat{\omega}_1'(E_1)$.
4. With $\widetilde{\sigma}_3(\widetilde{E}_3)$ and $\widehat{E}_2(\widetilde{E}_1)$, follow Steps 1 to 6 of Table 2 to obtain the uniform spline function $\widehat{\omega}_3'(E_3)$.
5. Compute the error $\widehat{err}(\overline{E}_1)$ for the $N_1 + 1$ strain values $\overline{E}_1$ using Eq. (66).
6. Minimize the function (67) to find the values of the parameters with which Eqs. (63), (64) and (65) are best fitted.

Table 3: Computational procedure for the case of Section 3.1.3

### *3.2. Determination of* $\omega_{13}$

Throughout previous subsections, according to the available test data or the user's priorities, we have seen the procedures to obtain the first derivative

of functions $\omega_1$ and $\omega_3$. So, in every case, only the first derivative function $\omega'_{13}$ remains to be determined in order to have the stored energy function of Eq.(14) completely defined. That is the purpose of this section.

*3.2.1. Pure shear test*

One of the possible tests that can be used to obtain the remaining function $\omega'_{13}$ is a specific biaxial test, see Figures 5(a) and 5(b). The biaxial test is performed in material (and spatial) principal directions $\boldsymbol{N}_1$ and $\boldsymbol{N}_3$, direction $\boldsymbol{N}_1$ being loaded in tension and direction $\boldsymbol{N}_3$ in compression. We regard a plane stress state in which the faces of the body normal to the direction $\boldsymbol{e}_2$ are free of tractions. The material fibers are initially oriented at $45^o$ (direction $\boldsymbol{a}_0$) with respect to the principal material axes. In this way, a pure shear state for strains and stresses may be analyzed using the system of representation $\boldsymbol{X}_{pr}$, see Figures 5(c) and 5(d), and the shear energy term $\omega_{13}$ may be easily calculated. The experimental measures give the points $(\widetilde{\lambda}, \widetilde{\sigma})$ or, equivalently, the distribution $\widetilde{\sigma}(\widetilde{E})$, where $\widetilde{\sigma}$ is the normal Cauchy stress acting on the face normal to $\boldsymbol{N}_1$ and $\widetilde{E} = \ln \widetilde{\lambda}$ is the longitudinal logarithmic strain in that direction. In direction $\boldsymbol{N}_3$, the stretch $\lambda_3 = 1/\lambda$ is imposed.

In the homogeneous deformation state depicted in Figure 5, the Hencky strain tensor $\boldsymbol{E}$ expressed in the basis of material principal stretches $\{\boldsymbol{N}_i\}$ is:

$$[\boldsymbol{E}]_{\boldsymbol{N}} = \ln [\boldsymbol{U}]_{\boldsymbol{N}} = \begin{bmatrix} \ln\lambda & 0 & 0 \\ 0 & \ln 1 & 0 \\ 0 & 0 & \ln\dfrac{1}{\lambda} \end{bmatrix} = \begin{bmatrix} E & 0 & 0 \\ 0 & 0 & 0 \\ 0 & 0 & -E \end{bmatrix} \tag{68}$$

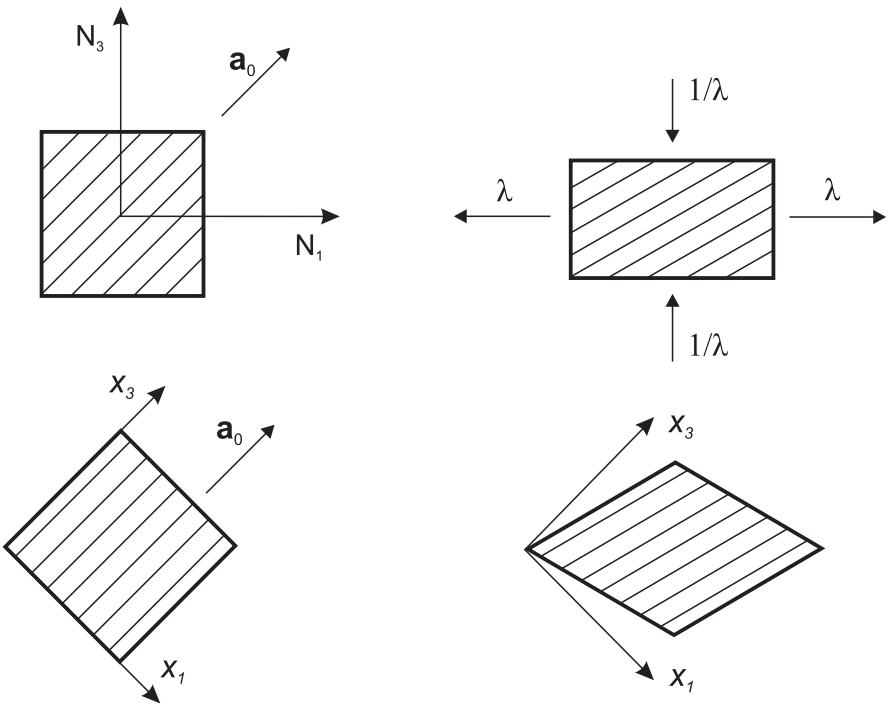


Figure 5: From left upper corner clockwise: (a) Reference configuration represented in principal strain basis $\{\boldsymbol{N}_i\}$. (b) Kinematics of deformation in the biaxial test, with corresponding principal stretches. (c) State of deformation (pure shear state) viewed in material reference frame $\boldsymbol{X}_{pr}$. (d) Reference configuration represented in $\boldsymbol{X}_{pr}$. $\boldsymbol{a}_0$ indicates the orientation of the preferred material direction (clockwise 45 degrees with respect to the compression principal direction).

where the result $\lambda_2 = 1$ emerges as a consequence of the isochoric motion being imposed on the plane $\{\boldsymbol{N}_1, \boldsymbol{N}_3\}$ and the incompressibility constraint $\lambda_1\lambda_2\lambda_3 = 1$. The pure shear state is clearly seen when this strain tensor is

represented in the basis $\boldsymbol{X}_{pr}$

$$[\boldsymbol{E}]_{\boldsymbol{X}_{pr}} = \begin{bmatrix} 0 & 0 & \ln\lambda \\ 0 & 0 & 0 \\ \ln\lambda & 0 & 0 \end{bmatrix} = \begin{bmatrix} 0 & 0 & E \\ 0 & 0 & 0 \\ E & 0 & 0 \end{bmatrix} \tag{69}$$

where the only non-zero logarithmic strain that takes part in the strain energy function given in Eq.(14) is the shear strain $E_{13} = \ln\lambda = E$.

Next, for each experimental measure $\widetilde{E} = \ln\widetilde{\lambda}$, we can obtain the associated Generalized Kirchhoff stress tensor $\boldsymbol{T}$ from

$$\boldsymbol{T} = \frac{\partial \mathcal{W}}{\partial \boldsymbol{E}} + p\boldsymbol{I} \tag{70}$$

where the hydrostatic pressure $p$ can be calculated from the plane stress condition:

$$\widetilde{\sigma}_2 = \widetilde{T}_2 = 0 = \omega_1'(\widetilde{E}_2) + p \implies p = -\omega_1'(\widetilde{E}_2) = -\omega_1'(0) = 0 \tag{71}$$

Thus, the tensor $\boldsymbol{T}$ is:

$$[\boldsymbol{T}]_{\boldsymbol{X}_{pr}} = \begin{bmatrix} 0 & 0 & \omega_{13}'(\widetilde{E}) \\ 0 & 0 & 0 \\ \omega_{13}'(\widetilde{E}) & 0 & 0 \end{bmatrix} \tag{72}$$

Note that the strain-like pure shear state shown in Figure 5(c), Eq.(69),

which results from the homogeneous biaxial deformation shown in Figure 5(b), Eq.(68), only leads to a stress-like pure shear state, Eq.(72), if the initial orientation of the anisotropic direction $\boldsymbol{a}_0$ (axis $\boldsymbol{e}_3$ of $\boldsymbol{X}_{pr}$) is as shown in Figure 5. In general, for other fiber orientations, the pure shear state for stresses is not obtained. Clearly, this is the logical extension to large strains of the mechanical behavior that is obtained for small strains, which arises due to the use of logarithmic strain measures and the uncoupled energy function given in Eq.(14).

Furthermore, in this particular case, the principal directions of strains and stresses are coincident, which are $\boldsymbol{N}_1$ and $\boldsymbol{N}_3$, so strain and stress tensors commute and $\boldsymbol{T}$ is also coincident with $\boldsymbol{\sigma}$. Then, the Cauchy stress tensor in the basis of principal stretches is

$$[\boldsymbol{\sigma}]_{\boldsymbol{N}} = \begin{bmatrix} \omega'_{13}(\widetilde{E}) & 0 & 0 \\ 0 & 0 & 0 \\ 0 & 0 & -\omega'_{13}(\widetilde{E}) \end{bmatrix} = \begin{bmatrix} \widetilde{\sigma}(\widetilde{E}) & 0 & 0 \\ 0 & 0 & 0 \\ 0 & 0 & -\widetilde{\sigma}(\widetilde{E}) \end{bmatrix} \tag{73}$$

where the stress in direction $\boldsymbol{N}_3$ predicted by our model is $\sigma_3(E_3) = -\sigma(E)$. Hence, the first derivative of the strain energy term $\omega_{13}$ can be calculated from the measured stress data points as

$$\omega'_{13}(\widetilde{E}) = \widetilde{\sigma}(\widetilde{E}) \tag{74}$$

Note that a uniaxial test with the fibers oriented at $45^o$ with respect to the

load direction would not be a valid test to obtain the function $\omega_{13}$ independently of the functions $\omega_1$ and $\omega_3$, because in that case there exists a coupling between longitudinal and shear strain components, even for the small strains case, as explained in Reference [21].

The procedure to determine the spline function $\omega'_{13}(E_{13})$ is summarized in Table 4. Unlike the previous cases, where tension and compression data points were necessary, we only need experimental data points for $\overline{E} > 0$. In this case, before constructing the odd spline function of the strains $\omega'_{13}(E_{13})$, the calculation $\widetilde{\sigma}(-\widetilde{E}) = -\widetilde{\sigma}(\widetilde{E})$ is performed for every strain $\widetilde{E} > 0$.

**Calculation of** $\omega'_{13}(E_{13})$

1. Experimental data: $\widetilde{\sigma}(\widetilde{E})$ from a biaxial test like the shown in Figures 5(a) and 5(b).
2. Perform the operation $\widetilde{\sigma}(-\widetilde{E}) = -\widetilde{\sigma}(\widetilde{E})$ for each value $\widetilde{E} > 0$.
3. Build (non-uniform) piecewise spline function $\sigma(E)$ from points $\widetilde{\sigma}(\widetilde{E})$.
4. Divide the domain $[-\widetilde{E}_{max}, \widetilde{E}_{max}]$ into $N$ uniform intervals with $N + 1$ equally spaced points $\overline{E}$.
5. Calculate the value $\omega'_{13}(\overline{E}_{13}) = \sigma(\overline{E})$ for all the strain points $\overline{E}_{13} = \overline{E}$.
6. Build uniform spline function $\omega'_{13}(E_{13})$ from all the values $\omega'_{13}(\overline{E}_{13})$.

Table 4: Computational procedure for the case of Section 3.2.1

*3.2.2. Simple shear test*

Other test from which it is possible to determine the derivative of the shear density energy function $\omega_{13}$ is the Simple Shear Test, see Figure 6(a). We consider a plane stress state throughout the incompressible specimen being tested in the sense that the faces of the body normal to the direction $\boldsymbol{e}_2$ are free of surface tractions, being the sheet embedded in the plane defined

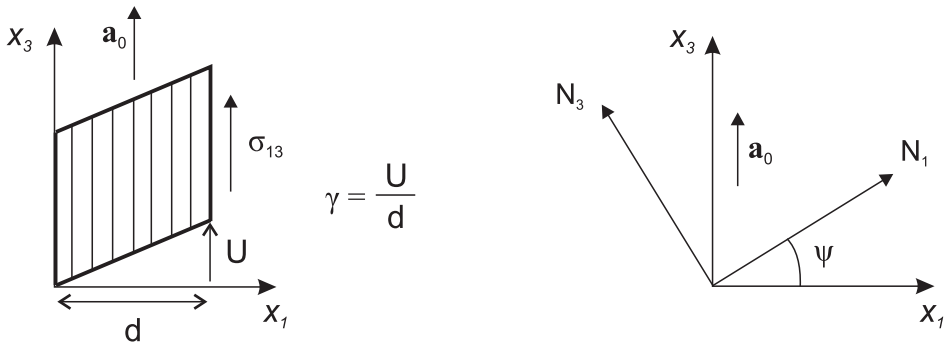


Figure 6: Left (a), kinematics of deformation in the simple shear test. Right (b), orientation of the principal material directions $\boldsymbol{N}_i$ and definition of angle $\psi\,(\gamma)$. $\boldsymbol{a}_0$ indicates the material orientation of the preferred anisotropic direction.

by the transversely isotropic direction $\boldsymbol{e}_1$ and the preferred direction $\boldsymbol{e}_3$, both defined in the reference configuration. In this case, the experimental measures give the points $(\widetilde{\gamma}, \widetilde{\sigma}_{13})$ or, equivalently, the distribution $\widetilde{\sigma}_{13}(\widetilde{\gamma})$, where $\widetilde{\sigma}_{13}$ is the shear stress acting on the face normal to $\boldsymbol{e}_1$ and $\widetilde{\gamma}$ the corresponding amount of shear strain.

In the homogeneous simple shear state depicted in Figure 6(a), the Hencky strain tensor $\boldsymbol{E}$ in the basis of Lagrangian principal directions $\{\boldsymbol{N}_i\}$ adopts the following form:

$$[\boldsymbol{E}]_{\boldsymbol{N}} = \begin{bmatrix} \ln\dfrac{1}{\lambda} & 0 & 0 \\ 0 & \ln 1 & 0 \\ 0 & 0 & \ln\lambda \end{bmatrix} = \begin{bmatrix} -\ln(\tan\psi) & 0 & 0 \\ 0 & 0 & 0 \\ 0 & 0 & \ln(\tan\psi) \end{bmatrix} \tag{75}$$

where the logarithmic strain in direction $\boldsymbol{e}_2$ is zero and $\lambda = \tan\psi$, being $\psi = 1/2\arctan(2/\gamma)$ the angle shown in Figure 6(b). The unit vectors $\{\boldsymbol{e}_i\}$,

which define the system of representation $\boldsymbol{X}_{pr}$, are expressed in the basis $\{\boldsymbol{N}_i\}$ as:

$$[\boldsymbol{e}_1, \boldsymbol{e}_2, \boldsymbol{e}_3]_{\boldsymbol{N}} = \begin{bmatrix} \cos\psi & 0 & \sin\psi \\ 0 & 1 & 0 \\ -\sin\psi & 0 & \cos\psi \end{bmatrix} \tag{76}$$

so, the logarithmic strains that take part in the strain energy function given in Eq.(14) are:

$$E_1(\psi) = \boldsymbol{E} : \boldsymbol{e}_1 \otimes \boldsymbol{e}_1 = -\ln(\tan\psi)\cos(2\psi) \tag{77}$$

$$E_2(\psi) = \boldsymbol{E} : \boldsymbol{e}_2 \otimes \boldsymbol{e}_2 = 0 \tag{78}$$

$$E_3(\psi) = \boldsymbol{E} : \boldsymbol{e}_3 \otimes \boldsymbol{e}_3 = \ln(\tan\psi)\cos(2\psi) = -E_1 \tag{79}$$

$$E_{13}(\psi) = \boldsymbol{E} : \boldsymbol{e}_1 \otimes \boldsymbol{e}_3 = -\ln(\tan\psi)\sin(2\psi) \tag{80}$$

$$E_{23}(\psi) = \boldsymbol{E} : \boldsymbol{e}_2 \otimes \boldsymbol{e}_3 = 0 \tag{81}$$

Note that $E_{12}(\psi)$ is also zero by definition of the reference frame $\boldsymbol{X}_{pr}$.

With these expressions known for each experimental measure $\gamma = \widetilde{\gamma}$, or equivalently $\psi = \widetilde{\psi}$, we can now obtain the corresponding components of the Generalized Kirchhoff stress tensor $\boldsymbol{T}$ from Eq.(70), where the hydrostatic pressure $p$ can be calculated again from the plane stress condition:

$$\widetilde{\sigma}_2 = \widetilde{T}_2 = 0 = \omega_1'(\widetilde{E}_2) + p \implies p = -\omega_1'(\widetilde{E}_2) = -\omega_1'(0) = 0 \tag{82}$$

The symmetric tensor $\boldsymbol{T}$ expressed in the material reference frame $\boldsymbol{X}_{pr}$ is, then:

$$[\boldsymbol{T}]_{\boldsymbol{X}_{pr}} = \begin{bmatrix} \omega_1'(\widetilde{E}_1) & 0 & \omega_{13}'(\widetilde{E}_{13}) \\ 0 & 0 & 0 \\ \omega_{13}'(\widetilde{E}_{13}) & 0 & \omega_3'(\widetilde{E}_3) \end{bmatrix} \tag{83}$$

where $\omega_{13}'(\widetilde{E}_{13})$ is undetermined and the values $\omega_1'(\widetilde{E}_1)$ and $\omega_3'(\widetilde{E}_3)$ can be computed evaluating the previously calculated spline functions $\omega_1'$ and $\omega_3'$ at points given by Eqs. (77) and (79), respectively. Representing now $\boldsymbol{T}$ in the principal deformation basis $\{\boldsymbol{N}_i\}$, we can apply the relationship (29) for $i \neq j$ in order to obtain the Rotated Cauchy stress tensor $\overline{\boldsymbol{\sigma}}$ expressed in that system of representation. Then, with $\overline{\boldsymbol{\sigma}}$ expressed in the basis $\{\boldsymbol{e}_i\}$, the push-forward operation $\boldsymbol{\sigma} = \boldsymbol{R}\overline{\boldsymbol{\sigma}}\boldsymbol{R}^T$ defined by the rotation tensor

$$[\boldsymbol{R}]_{\boldsymbol{X}_{pr}} = \begin{bmatrix} \sin(2\widetilde{\psi}) & 0 & -\cos(2\widetilde{\psi}) \\ 0 & 1 & 0 \\ \cos(2\widetilde{\psi}) & 0 & \sin(2\widetilde{\psi}) \end{bmatrix} \tag{84}$$

gives an expression for the experimental measures $\widetilde{\sigma}_{13}(\widetilde{\gamma})$, or equivalently $\widetilde{\sigma}_{13}(\widetilde{E}_{13})$, as a function of $\omega_1'(\widetilde{E}_1)$, $\omega_3'(\widetilde{E}_3)$, $\omega_{13}'(\widetilde{E}_{13})$ and $\widetilde{\psi}$. This last expression gives the desired value of the derivative $\omega_{13}'(\widetilde{E}_{13})$, namely:

$$\omega_{13}'(\widetilde{E}_{13}) = \frac{\widetilde{\sigma}_{13}(\widetilde{E}_{13}) - \frac{1}{2}\left[\omega_1'(\widetilde{E}_1) - \omega_3'(\widetilde{E}_3)\right]\left[\cos 2\widetilde{\psi} + \widetilde{E}_{13}\sin(2\widetilde{\psi})\right]\sin(2\widetilde{\psi})}{\sin^2(2\widetilde{\psi})(1-\widetilde{E}_1)} \tag{85}$$

Note that in this case, unlike for the pure shear test explained above,

there exists a coupling between the energy density shear term $\omega_{13}$ and the longitudinal contributions $\omega_1$ and $\omega_3$. Moreover, focusing on the expression appearing in the denominator of Equation (85), which is zero for $E_1 = 1$, one can view a limitation of this procedure to obtain the function $\omega_{13}$. Indeed, using Equations (77) and (80), it can be shown [22] that for the particular deformation state (value of $\gamma$) for which $E_1 = 1$, the shear logarithmic strain $E_{13}$ reaches a maximum, unlike the amount of shear strain $\gamma$ or the Green-Lagrange shear strain $\gamma/2$, which are monotonically increasing with the deformation evolution. Thus, from this test we can only determine the function $\omega_{13}$ between $E_{13} = 0$ and the maximum value reached by $E_{13}$, or equivalently, between the corresponding values taken by the longitudinal strain $E_1$, i.e. $E_1 = 0$ and $E_1 = 1$. On the other hand, if $\psi \simeq \pi/4$, Equation (85) results in $T_{13}(E_{13}) = \omega'_{13}(E_{13}) \simeq \sigma_{13}(E_{13})$, which is an expected result due to the fact that $\sigma_{13} \simeq \overline{\sigma}_{13} \simeq T_{13}$ for the small strain case.

From all the values $\omega'_{13}(\widetilde{E}_{13})$, calculated using Eq. (85) for all test data points $\widetilde{\gamma}$, the spline representation $\omega'_{13}(E_{13})$ is finally built. For convenience, the procedure is summarized in Table 5. In the given procedure, it is assumed that the functions $\omega'_1(E_1)$ and $\omega'_3(E_3)$ have been previously calculated. As before, symmetry considerations are taken into account before constructing the spline function $\omega'_{13}(E_{13})$.

**Calculation of $\omega'_{13}(E_{13})$**

1. Experimental data: $\widetilde{\sigma}_{13}(\widetilde{\gamma})$ from a simple shear test performed in the plane $\{x_1, x_3\}$ with $\gamma > 0$.
2. Compute angle $\widetilde{\psi} = \psi(\widetilde{\gamma}) = 1/2 \arctan(2/\widetilde{\gamma})$ and strain $\widetilde{E}_{13} = E_{13}(\widetilde{\psi})$ from Eq. (80) for each measure $\gamma = \widetilde{\gamma}$. Take $\psi(0) = \frac{\pi}{4}$.
3. Calculate $\widetilde{\sigma}_{13}(-\widetilde{E}_{13}) = -\widetilde{\sigma}_{13}(\widetilde{E}_{13})$ and $\widetilde{\psi}(-\widetilde{E}_{13}) = \dfrac{\pi}{2} - \widetilde{\psi}(\widetilde{E}_{13})$ for each $\widetilde{E}_{13} > 0$.
4. Build (non-uniform) piecewise spline functions: $\sigma_{13}(E_{13})$ from points $(\widetilde{E}_{13}, \widetilde{\sigma}_{13})$ and $\psi(E_{13})$ from $(\widetilde{E}_{13}, \widetilde{\psi})$.
5. Divide the domain $[-\widetilde{E}_{13max}, \widetilde{E}_{13max}]$ into $N$ uniform intervals with $N+1$ equally spaced points $\overline{E}_{13}$.
6. Calculate the $N+1$ values $\omega'_{13}(\overline{E}_{13})$ through Eq. (85) using splines $\sigma_{13}(E_{13})$, $\psi(E_{13})$, $\omega'_1(E_1)$ and $\omega'_3(E_3)$. Strains $E_1(\overline{\psi})$ and $E_3(\overline{\psi})$ are obtained from Eqs. (77) and (79).
7. Build the uniform spline function $\omega'_{13}(E_{13})$ from all the values obtained in the two previous steps.

Table 5: Computational procedure for the case of Section 3.2.2

## 4. Examples

In order to demonstrate the possibilities and applicability of the model, we have selected three examples. The first one shows that the Sussman-Bathe model for isotropic materials [17] is recovered as a special case of the present model. Then, predictions for the uniaxial tensile tests of transversely isotropic calendered rubber sheets published by Diani et al. [23] are given, and a comparison with a typical formulation based on a strain-energy function expressed in terms of invariants [24] is made. Finally, the experimental curves obtained by Morrow et al. [25] from skeletal muscle tissue are also predicted using our model. We want to note that if this last experimental work contained full compression-tension measures from the uniaxial tests, then

the minimum set of experimental results needed to completely determine the strain energy function given in Eq. (14) using the procedures detailed above would be available. However, only tensile data are provided, so some assumptions regarding the compression behavior will be made in order to define the model.

*4.1. Incompressible isotropic hyperelastic materials*

For isotropic materials, the free-energy may be formulated in the principal directions of the logarithmic strain tensor $\boldsymbol{E}$, see Eq. (10), and only one function needs to be determined from the experimental data, namely $\omega\left(E_i\right)$. Sussman and Bathe show how to obtain the derivative of this function by means of spline interpolations from the measured data points $\widetilde{\sigma}(\widetilde{E})$ of a compression-tension uniaxial test.

Their model is exactly recovered by our model when the given tests correspond, effectively, to an isotropic material. Indeed, the three cases detailed above in Sections 3.1.1, 3.1.2 and 3.1.3 converge to a single case when $\omega_1 = \omega_3 = \omega$. This is easily shown considering that, if the material being tested is incompressible and isotropic, to the experimental measures $\widetilde{\sigma}_1(\widetilde{E}_1)$ we can also add the linear relations $\widetilde{E}_2 = \widetilde{E}_3 = -\widetilde{E}_1/2$ for the transverse strains (with $1, 2, 3$ any orthogonal set of directions). Then compatibility Equations (44), (55) and (64) are always identically satisfied. Aside, since $\omega_1 = \omega_3$, Equations (43), (51), (63) and (65) converge to the same equation and the procedures given in the above sections are completely equivalent.

Moreover, since the free energy is formulated in principal directions for every deformation state, it is not necessary to consider the function $\omega_{13}(E_{13})$. Hence, we can conclude that the incompressible isotropic hyperelastic spline-based model is a particular case of the transversely isotropic model presented herein.

An illustrative example for this type of materials is provided by Sussman & Bathe. The considered tension-compression stress distribution, defined in the logarithmic strain range $-2 \leq E \leq 2$, is given by

$$\sigma(E) = 2\sinh(3E)(1 + 0.2\sin(10E)) + 2\sinh(1.5E)(1 - 0.2\sin(5E)) \quad (86)$$

The prediction given by our model, following the procedure detailed in Table 1 and taking as initial data the transverse strain distribution $E_2(E_1) = -E_1/2$, is shown in Figure 7. As in Reference [17], no difference is observed between both lines. Obviously, the comparisons with the Ogden hyperelastic model performed in Ref. [17] and the conclusions reached therein are also applicable to our model.

*4.2. Incompressible transversely isotropic hyperelastic materials*

Diani et al. present in their work [23] experimental data from uniaxial tensile tests for a calendered rubber-like material revealing transverse isotropy with respect to the calendering direction. The observed stress-like anisotropy is of about 30% for a stretch ratio of 150%. The purpose of this section is to show that similar results to those obtained for isotropic mate-

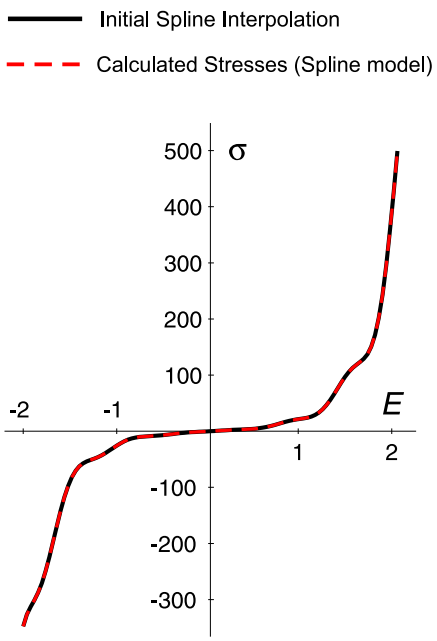


Figure 7: Example for incompressible isotropic material given in Ref. [17]. Initial piecewise spline interpolation of assumed data $\widetilde{\sigma}(\widetilde{E})$ and calculated stress using the transversely isotropic spline-based model. No difference is observed between both lines.

rials are obtained. A comparison with a strain-energy formulation based on (generalized) invariants developed by Itskov & Aksel [24] is also given. Obviously, the shear term $\omega_{13}$ can not be calculated with only this pair of uniaxial tests, being the behavior of the incompressible transversely isotropic material being tested not completely described by the given experimental data. Thus, with this example we show the accuracy of our model to reproduce some partial results and also how those results compare to the predictions obtained from the model of Itskov & Aksel.

The measured data points by Diani et al., along with several interpolations, are shown in Figure 8. As can be observed, the stresses calculated by

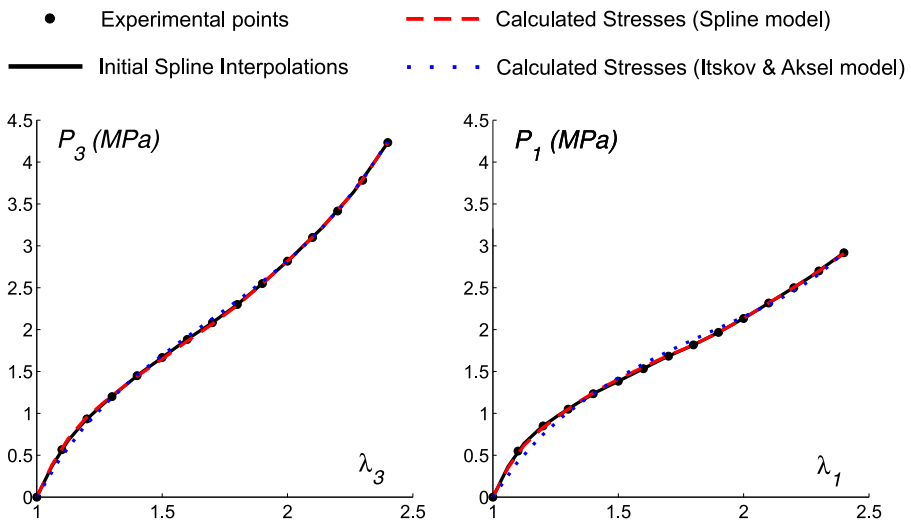


Figure 8: Measured nominal tension points $\widetilde{P}_3(\widetilde{\lambda}_3)$ and $\widetilde{P}_1(\widetilde{\lambda}_1)$ from uniaxial tests on calendered rubber in the anisotropic and transverse directions (Diani et al. [23]), their initial piecewise spline interpolations and calculated stresses using the Spline model (Section 3.1.3) and results from Itskov & Aksel (Ref. [24]). No appreciable difference is observed between stresses initially interpolated and subsequently calculated using the Spline model.

application of the methodology given in Section 3.1.3 (dashed lines) reproduce almost exactly the experimental measures in both directions. It can also be seen that, though the strain-energy function proposed by Itskov & Aksel gives a reasonable fit to the data, there is some disagreement between the prediction obtained from their model (dotted lines) and the exact spline interpolation (solid lines), being more noticeable within the lower stretch ranges ($1 < \lambda < 2$).

The experimental data by Diani et al. are given in terms of stretches ($\lambda_i$) and first Piola-Kirchhoff stresses ($P_i$), as shown in Figure 8 and hence the proper conversions have been previously performed ($E_i = \ln \lambda_i$; $\sigma_i = P_i \lambda_i$).

Furthermore, since Diani et al. only provide uniaxial tension measures, both stress distributions have been regarded odd functions of the corresponding strains in order to be able to use expressions such as Eq.(47) and Eq.(60). If compression measures had been available, they should have been employed instead and similar piecewise spline representations would have been obtained for the shown range ($\lambda > 1$).

The calculated stresses using our model have been obtained through Equations (49) and (62), which imply the simultaneous evaluation of functions $\omega_1$ and $\omega_3$. Hence, as explained in Section 3.1.3, the (least-squares) errors of the model are indeed included in the results represented in Figure 8, being almost imperceptible in this case. The transverse strain distribution $\widehat{E}_2(\widetilde{E}_1)$ defined in Section 3.1.3 has been assumed linear. If a linear distribution had not been realistic for the tested material, then the prediction of the data could possibly have not been so accurate. However, in that case, other more realistic non-linear transverse strain relations (cubic polynomial, exponential functions, etc.) could have been used instead in order to obtain good results again.

As a final example, we obtain a complete description of the strain energy function given in Eq. (14) from the set of three experimental curves measured from skeletal muscle tissue recently published by Morrow et al. [25]. As mentioned above, it will be necessary to assume the uniaxial compression behavior to be able to calculate all the stored energy function terms.

This type of biological material may be considered transversely isotropic

and hyperelastic. In addition, following the approach generally adopted in soft tissue mechanics, incompressible behavior is assumed. Morrow et al. tested the material through two uniaxial tests and a simple shear test, as described in Sections 3.1.3 and 3.2.2, respectively. In Figure 9, we present some points (positive values) extracted from the experimental curves that they provide. In order to make our plots comparable to those given in Ref. [25], the normal nominal stresses are represented as functions of the Green-Lagrange longitudinal strain measure $e = (\lambda^2 - 1)/2$, whereas the shear nominal stress is represented as a function of the shear strain measure $e = \tan\gamma$, being $\gamma$ the amount of shear strain defined in Section 3.2.2. With the proper strain and stress conversions previously performed, the procedures detailed in Tables 3 and 5 are applied. As in the previous example, only tension measures for the uniaxial tests are given. In this case, instead of freely specify a particular (antisymmetric) behavior for the compressive stretches, we have assumed compression stress distributions such as

$$\sigma_i\left(-E_i\right) = -k_i\sigma_i\left(E_i\right) \tag{87}$$

with $E_i \geq 0$ and $k_i > 0$, $i = 1, 3$. In that way, the least-squares method provides the set of globally stable energy functions $\omega_1$, $\omega_3$ and $\omega_{13}$ which "best" fits the originally measured positive stresses and the shape-assumed compression normal stresses. The two compression proportionality constants, i.e. $k_1$ and $k_3$, have been calculated as a part of the final solution of the

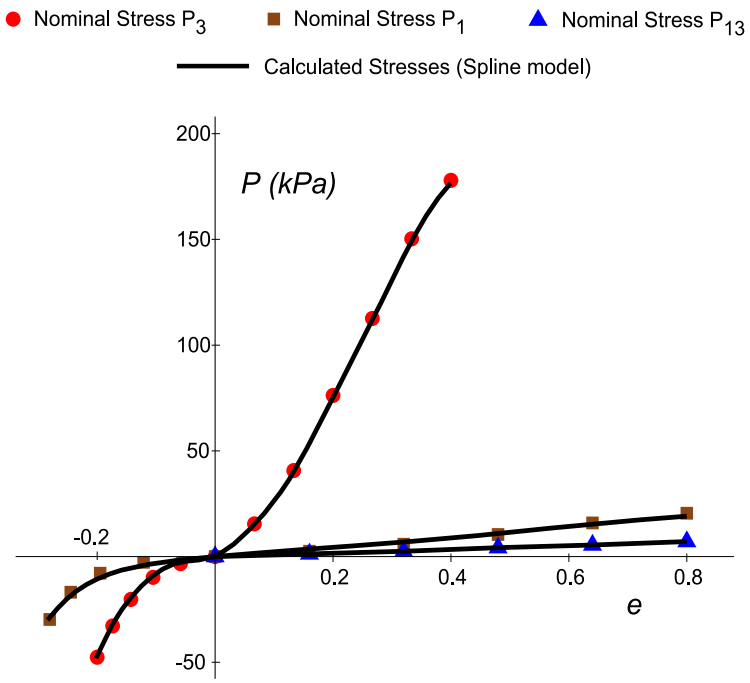


Figure 9: Predictions (solid lines) for the Morrow et al. [25] experiments (positive stress points) using the incompressible transversely isotropic spline-based model. First Piola-Kirchhoff normal tension stresses $\widetilde{P}_1$ and $\widetilde{P}_3$ and shear stresses $\widetilde{P}_{13}$ are obtained from the corresponding uniaxial tensile tests and a simple shear test, respectively. Compression normal stresses are calculated as a part of the procedure solution.

procedure. The obtained results are given in Figure 9. As before, the transverse strain distribution $\widehat{E}_2(\widetilde{E}_1)$ has been assumed linear. Finally, note that other uniaxial compressive behavior assumptions could have been regarded instead, giving as a result other set of spline-based stored energy function terms that would provide similar predictions for the real tension and new assumed compression stress distributions.

## 5. Conclusions

In this work we have extended the Sussman-Bathe spline-based model for incompressible isotropic hyperelasticity to transversely isotropic materials. This extension to incompressible transversely isotropic materials presents some extra difficulties and needed approximations which we have properly addressed. We have also shown that in practice, these approximations do not introduce relevant errors in the interpolation of the data. Several possible experimental sets have been considered in order to properly define the material behavior. For each possible set, the specific procedure to obtain the strain energy function has been detailed.

As shown, the model converges to the Sussman-Bathe model for the case of isotropy. Predictions for the transversely isotropic rubber-like hyperelastic material tested by Diani et al. are also given and compared to the predictions obtained from the hyperelastic model of Itskov and Aksel for this type of material. A description of our model is obtained using a set of three experimental curves as those given by Morrow et al. for skeletal muscle tissue if compression data is also included and assumed. We have shown that all these experiments are very accurately predicted by our model.

The procedure presents an attractive option for practical finite element modelling since the user has to simply supply some stress-strain data and the formulation is able to closely predict such behavior without sacrificing physical and mathematical correctness.

**Acknowledgements**

We acknowledge the anonymous reviewer #2 of the manuscript for providing a more elegant and accurate version of the inversion formula, Equation (40), than the one given in the original submission. Financial support for this work has been given by the Dirección General de Proyectos de Investigación of the Ministerio de Ciencia e Innovación and the Ministerio de Economía y Competitividad of Spain under grants DPI2008-05423 and DPI2011-26635.

**References**

[1] Bathe KJ. Finite Element Procedures. Prentice-Hall, New Jersey, 1996.

[2] Kojic M, Bathe KJ. Inelastic Analysis of Solids and Structures. Springer-Verlag, New York, 2005.

[3] Hasan OA, Boyce MC. Energy storage during inelastic deformation of glassy polymers. Polymer 1993;34:5085–92.

[4] Demiray H. A note on the elasticity of soft biological tissues. J Biomech 1972;5:309–11.

[5] Anand L. On H. Hencky's approximate strain-energy function for moderate deformations. J Appl Mech 1979;46:78–82.

[6] Anand L. Constitutive equations for hot-working of metals. Int J Plas 1985;1:213–31.

[7] Rolph WD, Bathe KJ. On a large strain finite element formulation for elasto-plastic analysis. In: Willam KJ, editor. Constitutive equations: macro and computational aspects. AMD, New York: ASME 1984;131–47.

[8] Hughes TJR, Winget J. Finite rotation effects in numerical integration of rate constitutive equations arising in large-deformation analysis. Int J Num Meth Eng 1980;15:1862–7.

[9] Simo JC, Pister KS. Remarks on rate constitutive equations for finite deformation problems: computational implications. Comp Meth Appl Mech Eng 1984;46:201.

[10] Truesdell C, Noll W. The non-linear field theories of mechanics. Handbuch der Physik, Vol. III/3, Springer, Berlin, New York.

[11] Ogden RW. Large deformation isotropic elasticity: on the correlation of theory and experiment for incompressible rubberlike solids. Proc R Soc Lond A 1972;326:565–84.

[12] Mooney M. A theory of large elastic deformation. J Appl Phys 1940;11:582–92.

[13] Rivlin RS. Large Elastic Deformations of Isotropic Materials. IV. Further Developments of the General Theory. Phil Trans R Soc Lond A 1948;241:379–97.

[14] Arruda EM, Boyce MC. A three-dimensional constitutive model for the large stretch behavior of rubber elastic materials. J Mech Phys Sol 1993;41:389–412.

[15] Blatz PJ, Ko WL. Application of finite elasticity theory to the deformation of rubbery materials. Trans Soc Rheol 1962;6:223–51.

[16] Yeoh OH. Characterization of elastic properties of carbon-black-filled rubber vulcanizates. Rub Chem Tech 1990;63:792–805.

[17] Sussman T, Bathe KJ. A Model of Incompressible Isotropic Hyperelastic Material Behavior using Spline Interpolations of Tension-Compression Test Data. Comm Num Meth Eng 2009;25:53–63.

[18] Valanis KC, Landel RF. The Strain-Energy Function of a Hyperelastic Material in Terms of the Extension Ratios. J Appl Phys 1967;38:2997–3002.

[19] Montáns FJ, Bathe KJ. Towards a model for large strain anisotropic elasto-plasticity. Chapter In: Onate E, Owen R, editors. Computational Plasticity. Springer-Verlag 2007:13–36.

[20] Montáns FJ, Bathe KJ. Computational issues in large strain elasto-plasticity. An algorithm for mixed hardening and plastic spin. Int J Num Meth Eng 2005;63:159–96.

[21] Jones RM. Mechanics of Composite Materials. New York, Taylor and Francis, 1999.

[22] Latorre M, Montáns FJ. On the interpretation of the logarithmic strain tensor in an arbitrary system of representation. To appear.

[23] Diani J, Brieu M, Vacherand JM, Rezgui A. Directional model for isotropic and anisotropic hyperelastic rubber-like materials. Mech Mater 2004;36:313–21.

[24] Itskov M, Aksel N. A class of orthotropic and transversely isotropic hyperelastic constitutive models based on a polyconvex strain energy function. Int J Sol Struct 2004;41:3833–48.

[25] Morrow DA, Donahue TLH, Odegard GM, Kaufman KR. Transversely isotropic tensile material properties of skeletal muscle tissue. J Mech Beh Biomed Mater 2010;3:124–29.